

1
2
3
4
5
6
7
8
9
10
11
12
13
14
15
16
17
18
19
20
21
22
23
24
25
26
27
28
29

Flatworm-specific transcriptional regulators promote the specification of tegumental progenitors in *Schistosoma mansoni*

George R Wendt¹, Julie NR Collins¹, Jimin Pei^{2,3}, Mark Pearson⁴, Hayley M. Bennett⁵, Alex Loukas⁴, Matt Berriman⁵, Nick V. Grishin^{2,3}, James J. Collins III^{1*}

¹Department of Pharmacology, UT Southwestern Medical Center, Dallas, Texas

²Department of Biophysics, Department of Biochemistry, University of Texas Southwestern Medical Center, Dallas, Texas

³Howard Hughes Medical Institute, University of Texas Southwestern Medical Center, Dallas, Texas

⁴Center for Biodiscovery and Molecular Development of Therapeutics, Australian Institute of Tropical Health and Medicine, James Cook University, Cairns, QLD, Australia.

⁵Wellcome Trust Sanger Institute, Wellcome Genome Campus, Hinxton, Cambridge, United Kingdom.

*To whom correspondence should be addressed

James J. Collins III
UT Southwestern Medical Center
Department of Pharmacology
6001 Forest Park. Rd.
Dallas, TX 75390
JamesJ.Collins@UTSouthwestern.edu

30 **Abstract**

31 Schistosomes infect more than 200 million people. These parasitic flatworms rely on a syncytial
32 outer-coat called the tegument to survive within the vasculature of their host. Although the
33 tegument is pivotal for their survival, little is known about maintenance of this tissue during the
34 decades schistosomes survive in the bloodstream. Here, we demonstrate that the tegument relies
35 on stem cells (neoblasts) to specify fusogenic progenitors that replace tegumental cells lost to
36 turnover. Molecular characterization of neoblasts and tegumental progenitors led to the discovery
37 of two flatworm-specific zinc finger proteins that are essential for tegumental cell specification.
38 These proteins are homologous to a protein essential for neoblast-driven epidermal maintenance
39 in free-living flatworms. Therefore, we speculate that related parasites (i.e., tapeworms and flukes)
40 employ similar strategies to control tegumental maintenance. Since parasitic flatworms infect
41 every vertebrate species, understanding neoblast-driven tegumental maintenance could identify
42 broad-spectrum therapeutics to fight diseases caused by these parasites.

43

44 **Introduction**

45 Schistosomes cause significant morbidity and mortality in some 200 million people in the
46 developing world (Hotez and Fenwick 2009). An astounding feature of these parasites is their
47 ability to survive for decades in the vasculature of their human hosts. Indeed, the literature is rife
48 with cases of patients harboring reproductively active schistosomes 20-30 years after leaving
49 endemic regions (Harris et al. 1984, Hornstein et al. 1990, Payet et al. 2006). How these parasites
50 flourish for years in what has been described as “the most hostile environment imaginable”
51 (McLaren 1980) remains an open question. A skin-like tissue known as the tegument is thought to
52 be key for the schistosome’s long-term survival inside the vasculature of the host. The tegument
53 is a continuous syncytium that covers the worm’s entire outer surface. While the tegument itself
54 lacks many basic cellular components (i.e., ribosomes, nuclei, endoplasmic reticulum), this tissue
55 is connected via cytoplasmic projections to thousands of individual cell bodies that lay beneath the
56 parasite’s muscle layers. These tegumental cell bodies (called “cytons” in the classic literature)
57 are nucleated and provide a continuous stream of proteins and secreted material to support
58 tegumental function (Wilson and Barnes 1974, McLaren 1980). Scientists have long thought that
59 the uninterrupted architecture of the tegument and the unique molecular composition of the
60 tegumental surface, are key for evasion of host defenses and parasite survival (McLaren 1980,
61 Skelly and Wilson 2006). Despite these essential functions, little is known on the cellular and
62 molecular level about the development and long-term maintenance of the tegument inside the
63 parasite’s definitive host.

64 Schistosomes are members of the Neodermata (Ehlers 1985, Littlewood and Bray 2001,
65 Laumer et al. 2015), a large clade of parasitic Platyhelminthes that includes some of nature’s most
66 notorious pathogens, including both tapeworms and some 20,000 species of flukes. Aside from

67 being parasites, all members of the Neodermata are united by the fact that they possess a tegument
68 similar to that of the schistosome. As in schistosomes, the importance of this tegument in the
69 biology of these parasites cannot be overstated. The tegument forms a protective barrier that guards
70 these parasites, not only against the host immune system, but also from the physical extremes they
71 encounter living in the digestive system, blood, or internal organs of their host. The tegument also
72 serves as a conduit for the worms to acquire nutrients (Halton 1997). Indeed, during the course of
73 evolution, tapeworms have lost their gut in favor of utilizing the tegument as their primary means
74 of nutrient acquisition. Moreover, the tegument is rapidly remodeled on a cellular and molecular
75 level when these parasites transition between intermediate and definitive hosts (Hockley and
76 McLaren 1973, Tyler and Tyler 1997, Tyler and Hooke 2004), suggesting that this tissue may also
77 have been pivotal in allowing the complex multi-host lifecycles that are essential for the
78 propagation of these obligate parasites. Given the benefits that the tegument affords these
79 parasites, and its absence in free-living members of the phylum, it is widely credited as the key
80 innovation leading to the evolution of parasitism in the Platyhelminthes (Tyler and Tyler 1997,
81 Tyler and Hooke 2004, Littlewood 2006, Laumer et al. 2015). Thus, a deeper understanding of
82 the molecular regulation of tegument development could provide important insights into flatworm
83 evolution and suggest targets for the development of novel anthelmintics.

84 Upon invasion of their definitive host, the schistosome tegument is rapidly remodeled in
85 a process that appears to be fueled by the fusion of mesenchymal cells to the outer tegument
86 (Hockley and McLaren 1973, Skelly and Shoemaker 2001). After this fusion takes place,
87 however, little is known about how the cellular composition of the tegument changes during
88 parasite maturation or during the decades that these parasites can potentially live in the
89 vasculature. One important, but virtually unexplored, question is whether the tegument is subject

90 to physiological cell replenishment or turnover. Since the tegument is a syncytium, it is possible
91 that aberrant function (or death) of a small fraction of cells could be compensated for by the
92 remaining cells in the tissue. While this possibility has not been ruled out, recent studies have
93 hinted at a role for stem cells (called neoblasts (Collins et al. 2013)) in contributing to the
94 rejuvenation and maintenance of the schistosome tegument (Collins et al. 2016). Indeed, the
95 primary differentiation output of neoblasts appears to be a group of short-lived cells that express
96 an mRNA encoding TSP-2, a promising anti-schistosome vaccine candidate that is present at
97 high-levels in the tegument (Tran et al. 2006, Pearson et al. 2012) and on tegument-derived
98 extracellular vesicles (Sotillo et al. 2016). In addition to expressing *tsp-2* mRNA, these neoblast
99 progeny cells express a collection of known tegument-specific factors, suggesting that neoblasts
100 are important in some capacity for contributing to the maintenance of the tegument (Collins et al.
101 2016). However, due to a lack of tools for visualizing both the outer tegument and its attached
102 cell bodies, the relationship between *tsp-2*⁺ neoblast progeny and the tegument remains
103 uncharacterized.

104 Here, we describe a novel methodology to fluorescently label the schistosome tegument
105 and demonstrate that tegumental cells are renewed continuously by a population of *tsp-2*⁺
106 progenitor cells that fuse with the tegument. To define how this process is regulated on a molecular
107 level, we characterized the transcriptomes of both neoblasts and tegumental progenitors using
108 fluorescence-activated cell sorting (FACS). Using these transcriptomes as a guide, we conducted
109 an RNAi screen to discover molecular regulators of tegument differentiation, and identify a pair
110 of flatworm-specific zinc finger proteins, called ZFP-1 and ZFP-1-1, that are essential for the
111 specification of new tegumental cells. Since these zinc finger proteins are flatworm-specific, and
112 a homolog of these proteins is known to be essential for a very similar epidermal biogenesis

113 program in free-living flatworms, we speculate that these genes are likely to be key for tegument
114 development across the Neodermata. Our data demonstrate a formal role for neoblasts in
115 tegumental maintenance and provide the first molecular insights into how tegumental fates are
116 specified.

117

118 **Results**

119

120 **The schistosome tegument and associated cell bodies can be labeled specifically with**
121 **fluorescently conjugated dextran**

122 A prerequisite for studying the development of the tegument is the ability to visualize both
123 the outer tegument and its associated cell bodies microscopically (Figure 1A). However, this
124 presently can only be accomplished by transmission electron microscopy (McLaren 1980), which
125 is not compatible with methodologies to visualize the expression of molecular markers. Therefore,
126 we explored a variety of live cell dyes and delivery techniques to identify an approach to
127 specifically label the schistosome tegument fluorescently (Figure 1A). We found that soaking live
128 parasites in a hypotonic solution of 10 kDa fluorescent dextran specifically labeled the tegument
129 surface (Figure 1B), cytoplasmic projections (Figure 1C), and the tegumental cell bodies (Figure
130 1D) that sit beneath the parasite's body wall muscles (Figure 1E, F). Since isotonic dextran
131 solutions failed to label the tegument, we suspect that specific labeling requires damage to the
132 outer tegumental membranes. Consistent with classic ultrastructural studies, these tegumental cell
133 bodies extend one or more projections towards the tegumental surface (Morris and Threadgold
134 1968, Hockley 1973) (Figure 1F) and appear to form an elaborate interconnected network of
135 cellular projections and cell bodies (Movie 1). Since the narrowest tegumental cytoplasmic
136 projections are much larger (~100 nm) (Hockley 1973) than the diameter of the fluorescent-dextran
137 conjugate, it is likely that this approach is capable of labeling all cells directly attached to the
138 tegument.

139

140

141 **Definitive tegumental cells express *calpain*, *npp-5*, *annexin* and *gtp-4* but not *tsp-2***

142 To study the development of the tegument, we next sought to identify molecular markers
143 expressed in tegumental cells and, therefore, performed fluorescence in situ hybridization (FISH)
144 experiments on dextran-labeled parasites. Examination of a panel of candidate tegument-specific
145 factors assembled from the literature (Skelly and Shoemaker 1996, van Balkom et al. 2005, Braschi
146 and Wilson 2006, Rofatto et al. 2009, Wilson 2012) found that mRNAs for *calp*, *npp-5*, *annexin*
147 and *gtp-4* were exclusively expressed in dextran positive cells at the level of the tegument (Figure
148 1G and Figure 1-Figure Supplement 1A-C), suggesting these genes encode markers of tegumental
149 cells. We previously demonstrated that cells expressing the mRNA for the tegument-specific
150 factor *tsp-2* are rapidly produced by neoblasts and then rapidly turned over (Collins et al. 2016).
151 Since a variety of proteomic and immunological studies have demonstrated that the TSP-2 protein
152 is associated with the tegument (van Balkom et al. 2005, Braschi and Wilson 2006, Tran et al.
153 2006, Pearson et al. 2012, Wilson 2012), we were surprised that virtually all *tsp-2* mRNA-
154 expressing cells were dextran-negative despite, in many cases, being found in close proximity to
155 dextran-labeled tegumental cell bodies (Figure 1H). Similarly, we did not observe extensive co-
156 localization of *tsp-2* with the tegumental markers *calpain*, *npp-5*, *annexin* and *gtp-4* in adult
157 parasites (Fig. 1I and Figure 1-Figure Supplement 1D-F). Indeed, extensive examination using
158 both tegumental markers and dextran labeling revealed only 5 tegumental cells that expressed low
159 levels of *tsp-2* from 3074 tegumental cells examined (~0.2%). We made similar observations with
160 another tegument-enriched factor *sm13* (Figure 1-Figure Supplement G-L; 1/1826 tegumental cells
161 was *sm13*⁺) that is exclusively expressed in *tsp-2*⁺ cells (Collins et al. 2016). Together, these data
162 suggest that *tsp-2* mRNA is not expressed at high-levels in definitive tegumental cells.

163

164 ***tsp-2*⁺ cells include putative progenitors to the definitive tegument**

165 To reconcile the observation that *tsp-2* is not highly expressed in the definitive tegument
166 with the extensive literature linking the TSP-2 protein to the tegument surface, we performed
167 immunofluorescence with an anti-TSP-2 antibody (Pearson et al. 2012). We verified the
168 specificity of this antibody by Western-blot following *tsp-2* RNAi treatment (Figure 1- Figure
169 Supplement 2A). Similar to previous studies (Tran et al. 2006, Pearson et al. 2012), we observed
170 high levels of TSP-2 protein localized on the tegumental surface (Figure 1- Figure Supplement
171 2B,C). Upon the optimization of labeling conditions, we also noted that TSP-2 protein could be
172 detected in *tsp-2* mRNA-expressing cell bodies and their projections which extend toward the
173 tegument surface (Figure 1J, Figure 1- Figure Supplement 2D). We also detected lower levels of
174 TSP-2 in tegumental cell bodies expressing a mixture of tegument-specific mRNAs (*annexin*, *gtp*-
175 *4*, *npp-5*, and *calp*) (Figure 1J) or labeled with dextran (Figure 1- Figure Supplement 2E).
176 Although lower levels of TSP-2 were typically found in tegumental cell bodies, higher levels of
177 the protein were observed on the apical sides of these cells and in the projections extending to the
178 tegument surface (Figure 1J, Figure 1-Figure Supplement 2D-E, Movie 2). Additionally, we
179 observed rare cells expressing markers of definitive tegumental cells, TSP-2 protein, and low
180 levels of *tsp-2* mRNA (Figure 1K). Based on these data, an attractive model is that *tsp-2* mRNA-
181 expressing cells include a population of tegumental precursors and that as these cells differentiate
182 to mature tegumental cells, the TSP-2 protein remains stable while the *tsp-2* mRNA is down-
183 regulated.

184 To explore the model that *tsp-2*⁺ cells include a population of tegumental precursors, we
185 examined the kinetics of the differentiation of neoblasts to *tsp-2*⁺ cells and tegumental cells by
186 performing pulse-chase experiments with the thymidine analog 5-Ethynyl-2'-deoxyuridine (EdU).

187 In these experiments, we injected schistosome-infected mice with EdU to label proliferative
188 neoblasts and then examined the kinetics by which these cells differentiate to produce both *tsp-2*⁺
189 and definitive tegumental cells. If *tsp-2*⁺ cells include precursors to the definitive tegument we
190 anticipate: (I) that EdU would chase into the nuclei of *tsp-2*⁺ cells prior to the definitive tegumental
191 cells and (II) that as EdU signal is lost from the *tsp-2*⁺ cell compartment we would observe a
192 concomitant increase in the fraction of EdU⁺ tegumental cells. Consistent with this model, at D3
193 following an EdU pulse 45% of *tsp-2*⁺ cells are EdU⁺, whereas just 0.1% of definitive tegumental
194 cells are EdU⁺ at this time point. After D3, however, the fraction of EdU⁺*tsp-2*⁺ cells began to
195 drop, and the fraction of EdU⁺ tegumental cells jumped to 12% by D5 before peaking at around
196 20% between D7 and D11 (Figure 1L-M). By D35 the fraction of EdU⁺ tegumental cells dropped
197 to 2.2%, suggesting that tegumental cells are subject to physiological turnover inside a mammalian
198 host. These data, together with our TSP-2 immunolabeling studies, are consistent with a model in
199 which neoblasts produce a population of short-lived *tsp-2*⁺ progenitor cells that differentiate and
200 fuse with the tegument. Thus, tegumental cells appear to rely on neoblasts for their continual
201 maintenance.

202 **FACs purification and molecular characterization of neoblasts and TSP-2⁺ cells**

203 As a first step towards understanding how tegument development and tissue homeostasis
204 is regulated on a molecular level, we set out to characterize the expression of genes in both
205 neoblasts and *tsp-2*⁺ cells. Although our previous work exploited the radiation sensitivity of
206 neoblasts and *tsp-2*⁺ cells to identify candidate cell-type specific markers (Collins et al. 2013,
207 Collins et al. 2016), we were interested in directly measuring gene expression in these cells. To
208 this end, we developed a FACS methodology to purify both proliferative neoblasts and TSP-2⁺
209 tegumental progenitors from single-cell suspensions of schistosome somatic tissues (Figure 2A).

210 Since schistosome neoblasts appear to be the only proliferative somatic cell type (Collins
211 et al. 2013), we adapted a methodology developed for FACS purifying neoblasts from free-living
212 planarian flatworms using the live cell DNA-binding dye Hoechst 33342 (Hayashi et al. 2006). In
213 this approach, S/G2/M phase neoblasts can be purified from non-cycling (2N DNA content) cells
214 due to their elevated DNA content ($> 2N$) as measured by Hoechst 33342 labeling intensity (Figure
215 2A). Tetraspanins are transmembrane proteins often localized to the cell surface (Charrin et al.
216 2014). Since our anti-TSP-2 antibody is directed to a putative extracellular loop of TSP-2 (Pearson
217 et al. 2012), we also employed this antibody to FACS purify TSP-2⁺ cells (Figure 2A). Performing
218 FACS on cell populations labeled with both Hoechst 33342 and anti-TSP-2, we could clearly
219 resolve cells with $>2N$ DNA content (putative neoblasts) and 2N cells with high levels of anti-
220 TSP-2 labeling (Figure 2B). Cells with $>2N$ DNA content possessed typical neoblast morphology
221 (small cells with a high nuclear:cytoplasmic ratio), whereas 2N cells with the highest levels of
222 TSP-2⁺ labeling possessed a lower nuclear:cytoplasmic ratio and labeled strongly for TSP-2 on
223 their surface (Figure 2C). We also noted a large population of cells with intermediate levels of
224 TSP-2 labeling (i.e., cells with 10^2 - 10^4 in relative TSP-2 labeling intensity, Figure 2B). Visual
225 examination of these cells found that they did not possess high levels of TSP-2 surface labeling.
226 Instead, these “TSP-2 Intermediate” cells had either no TSP-2 surface labeling or had pieces of
227 TSP-2-labeled debris attached to their surface (Figure 2-Figure Supplement 1). Since TSP-2 is
228 present at high-levels on the outer tegument, we believe these cells are falsely scored as TSP-2⁺
229 due to the contamination of TSP-2⁺ tegumental debris in our FACS preparations.

230 To unambiguously confirm the identity of the neoblast and TSP-2⁺ cell populations, we
231 also performed FACS with parasites 7 days post-treatment with 100 Gy of γ -irradiation, which is
232 sufficient to deplete both neoblasts and *tsp-2*⁺ cells but spare other differentiated cell types in the

233 worms (Collins et al. 2013, Collins et al. 2016). Both the neoblasts and TSP-2⁺ cell populations
234 are eliminated following irradiation, confirming the specificity of our sorting procedure (Figure
235 2B). We also FACS-purified 2N TSP-2⁻ irradiation insensitive cells, which we refer to hereafter
236 as “IR Rest” cells (Figure 2B). Consistent with the idea that the IR Rest cells represent various
237 differentiated cell types in the parasite, the FACS-purified cells displayed a range of cellular
238 morphologies (e.g., ciliated cells) and nuclear:cytoplasmic ratios (Figure 2C).

239 To define cell-type specific expression profiles, we performed RNAseq on purified
240 neoblasts, TSP-2⁺ cells, and IR Rest cell populations (Figure 2B-C). We performed pair-wise
241 comparisons to define relative differences in gene expression between these three cell populations
242 (Supplementary File 1) and used model-based clustering (Si et al. 2014) (Figure 2D) to identify
243 genes whose expression was specifically enriched in each cell population (Supplementary File 2).
244 From this clustering analysis, we found clusters of genes whose expression was enriched to varying
245 degrees in the IR Rest (clusters 1, 11, 15), neoblast (cluster 6 and to a lesser extent 10), and TSP-
246 2⁺ cell populations (cluster 3, 14, 5, 8). Examination of genes in these clusters identified
247 anticipated cell-type specific markers: the IR Rest-enriched cluster 15 included genes whose
248 expression is associated with differentiated cells such as neurons (i.e. *neuropeptide f receptor*,
249 *neuroendocrine protein 7b2*); the neoblast-enriched cluster 6 included known neoblast-specific
250 factors including *fgfrA*, *nanos2*, and a variety of cell cycle-associated regulators; and the TSP-2⁺-
251 enriched clusters 3, 14, 8 included *tsp-2* and a variety of genes previously shown to be expressed
252 in *tsp-2*⁺ cells including *sm13*, *sm25*, *cationic amino acid transporter*, and *dysferlin* (Figure 2E)
253 (Collins et al. 2016). We also identified clusters of genes whose expression was enriched in two
254 of the three cell populations. For instance, cluster 13 included genes enriched in both neoblasts
255 and TSP-2⁺ cells. Among the genes in cluster 13 was the *S. mansoni p53* homolog that was

256 previously demonstrated to be highly expressed in both neoblasts and *tsp-2*⁺ cells (Collins et al.
257 2016).

258 Since we found that TSP-2-labeled cells expressed tegument-enriched genes (Figure 1J,K)
259 we also reasoned that our FACS data might include markers of definitive tegument. Indeed, we
260 noted that the TSP-2-enriched cluster 5 included all four of our validated markers of definitive
261 tegumental cells (*calp*, *npp-5*, *annexin*, and *gtp-4*) (Figure 2E). To explore the significance of this
262 observation, we performed an *in-situ* hybridization screen to characterize the expression of genes
263 present in TSP-2-enriched clusters, giving specific attention to genes present in cluster 5.
264 Examining the expression of genes both at the level of the tegument and deeper inside the
265 parenchyma where most *tsp-2*⁺ cells reside (Figure 2F), we found that 26/28 genes in clusters 3,
266 14, 5, 8 that gave discernable expression patterns were expressed in either *tsp-2*⁺ cells or definitive
267 tegumental cells (Figure 2G, Figure 2-Figure Supplement 2,3, Supplementary File 3). Among
268 these genes, 15/20 in cluster 5 alone were expressed in definitive tegumental cells (Supplementary
269 File 3), suggesting that genes in this cluster appear to be enriched for tegument-specific transcripts.
270 We also noted from these analyses that *tsp-2*⁺ cells are heterogeneous on a molecular level: cells
271 deeper in the parenchyma tended to express a dynein heavy chain homolog (Figure 2G), whereas
272 more superficial *tsp-2*⁺ cells expressed *sm13* (Figure 2G) and *sm25* (Figure 2-Figure Supplement
273 2). Similarly, we found a pair of transcripts encoding Endophilin B1 homologs that were expressed
274 at high levels in a subset of mature tegumental cell bodies (Figure 2G). This heterogeneity could
275 highlight populations of cells at different stages of commitment to the tegumental lineage. Taken
276 together, these data suggest that clusters 3, 5, 8, 14 are enriched for transcripts expressed in either
277 *tsp-2*⁺ cells or definitive tegumental cells, providing an additional line of evidence connecting *tsp-*
278 *2*⁺ cells and the definitive tegument.

279 **An RNAi screen identifies *zfp-1* and *zfp-1-1* as potential regulators of tegument development**

280 To define genes that regulate the development of the tegument lineage, we used our
281 neoblast and TSP-2⁺-enriched datasets to select candidates for an RNAi screen of genes encoding
282 putative transcription factors, RNA binding proteins, signaling molecules, and schistosome
283 specific proteins. For this screen, we performed RNAi on adult parasites and examined the
284 numbers of neoblasts (by EdU-labeling) and *tsp-2*⁺ cells (by FISH) (Figure 3A). We reasoned that
285 genes required for general neoblast maintenance/proliferation would be essential for the
286 maintenance of both EdU⁺ neoblasts and *tsp-2*⁺ cells (e.g., *histone H2B* (Figure 3B)), whereas
287 genes important for tegument development would be essential for the maintenance of *tsp-2*⁺ cells
288 but dispensable for neoblast maintenance (Figure 3A). From these experiments, we identified
289 several factors essential for neoblast maintenance, including: a homolog of the human breast
290 cancer type 1 susceptibility protein (BRCA1), a homolog of the BRCA1 associated RING domain
291 1 (BARD1) protein, a previously uncharacterized fibroblast growth factor (FGF) receptor, and a
292 homolog of the p53 tumor suppressor (Figure 3B). A number of other genes were screened that
293 gave no stem cell or *tsp-2* phenotype (Figure 3-Figure Supplement 1). Given our focus on genes
294 required for tegumental differentiation, these genes were not explored further.

295 In addition, we found that RNAi of genes encoding two related C2H2 zinc finger proteins,
296 *zfp-1* and *zfp-1-1*, resulted in a reduction in the total number of *tsp-2*⁺ cells yet spared the number
297 of EdU-labeled neoblasts (Figure 3C). Indeed, RNAi-mediated transcript reduction of either *zfp-*
298 *1* or *zfp-1-1* (Figure 3-Figure Supplement 2) resulted in an approximately 50% reduction in the
299 number of *tsp-2*⁺ cells (Figure 3C,D) and led to no change in the total number of *nanos2*⁺ neoblasts
300 capable of incorporating EdU (Figure 3E,F). The effect of *zfp-1* and *zfp-1-1* RNAi treatment was
301 not specific to the expression of *tsp-2*⁺, as RNAi of either of these genes similarly led to a sizable
302 decrease in the total number of cells expressing *sm13*, a gene that is expressed in nearly all

303 superficial *tsp-2*⁺ cells (Figure 3G,H, Figure 3-Figure Supplement 2). These observations suggest
304 *zfp-1* and *zfp-1-1* are important for the differentiation and/or maintenance of *tsp-2*⁺ cells.

305 Consistent with our RNAseq data, we found that *zfp-1* was expressed exclusively in
306 *nanos2*⁺ neoblasts and not in *tsp-2*⁺ cells (Figure 3I,J). Conversely, *zfp-1-1* was not expressed in
307 *nanos2*⁺ neoblasts but was expressed at high levels in *tsp-2*⁺ cells (Figure 3K,L). Similar to other
308 transcripts enriched in *tsp-2*⁺ cells, *zfp-1-1* appeared to be expressed in a subset of *tsp-2*⁺ cells that
309 were located more internally within the parasite (Figure 3M) but not in more peripherally-located
310 *sm13*⁺*tsp-2*⁺ cells (Figure 3-Figure Supplement 3). Since neoblasts are typically located deeper
311 inside the parasite, these more internal *tsp-2*⁺*zfp-1-1*⁺ cells could represent early neoblast progeny,
312 whereas the peripheral *tsp-2*⁺*sm13*⁺ cells may represent more mature tegumental progenitors. We
313 further determined that *zfp-1-1* was not expressed in definitive tegumental cells (Figure 3L) and
314 that *zfp-1* and *zfp-1-1* were not co-expressed (Figure 3J; 0/64 *zfp-1-1* cells were *zfp-1*⁺). Thus, *zfp-*
315 *1* expression appears to be neoblast-specific, whereas *zfp-1-1* expression is enriched in a subset of
316 *tsp-2*⁺ cells.

317

318 ***zfp-1* and *zfp-1-1* are members of a family of flatworm-specific DNA binding proteins whose**
319 **homolog in planarians regulates epidermal lineage specification**

320 We examined the amino acid sequences of the proteins encoded by *zfp-1* and *zfp-1-1*. Not
321 only were the three C2H2 zinc finger domains of ZFP-1 and ZFP-1-1 highly similar to one another,
322 but we also uncovered closely-related C2H2 zinc finger domain-containing proteins in the
323 genomes of free-living (i.e., planarians and macrostomids) and parasitic flatworms (i.e., flukes,
324 tapeworms, monogeneans) (Figure 4A). A thorough examination of proteins from taxa outside the
325 Platyhelminthes failed to find any close relatives that shared both high sequence identity and a

326 similar number of C2H2 domains, suggesting that these proteins are likely to be flatworm specific.
327 Phylogenetic analysis of these proteins revealed two distinct groups of these ZFP-1 family
328 proteins: one group more similar to the schistosome *zfp-1* and another more closely related to *zfp-*
329 *1-1* (Figure 4B). Among the homologs identified was a protein encoded from the *zfp-1* gene in the
330 planarian *Schmidtea mediterranea*. In parallel to our model for tegument renewal by short-lived
331 *tsp-2⁺* tegumental progenitors, the planarian epidermis is perpetually rejuvenated from a
332 population of short-lived epidermal progenitors derived from the neoblasts (Eisenhoffer et al.
333 2008, van Wolfswinkel et al. 2014). The production of these epidermal progenitors relies on the
334 planarian *zfp-1*, which is expressed in a subset of lineage-restricted neoblasts (van Wolfswinkel et
335 al. 2014). Thus, our results with *zfp-1* and *zfp-1-1* suggest the potential for a conserved role for
336 these proteins in coordinating epidermal biogenesis programs among flatworms.

337 Although *zfp-1* has been previously characterized in *S. mediterranea*, the molecular
338 function of this group of novel proteins is not clear. Since we found proteins in this family shared
339 little homology outside the three C2H2 zinc finger domains, we reasoned that these domains are
340 likely key to the function of these proteins. C2H2 zinc finger domains are best known for their
341 ability to function as transcriptional regulators by binding DNA, however, these domains can also
342 participate in RNA-binding and protein:protein interactions (Krishna et al. 2003, Hall 2005, Brayer
343 and Segal 2008). Thus, we examined the sequences of these proteins in more detail. C2H2 zinc
344 finger domains contain two conserved cysteines and two conserved histidines for zinc-binding
345 (highlighted in black background in Figure 4A). For the *zfp-1* family proteins, we observed that
346 the residues between the second zinc-coordinating cysteine and the first zinc-coordinating histidine
347 of the second and third zinc fingers exhibited high sequence conservation, forming the motifs
348 QRSNLQR and RKDHLxR, respectively (Figure 4A). Typically, each C2H2 zinc finger interacts

349 with three consecutive DNA base pairs, and the first, fourth, and seventh positions in these motifs
350 (highlighted in cyan background in Figure 4A) are key contributors to the binding specificity of
351 the 3' base, the middle base, and 5' base of the primary interaction DNA strand, respectively
352 (Wolfe et al. 2000, Klug 2010). Given this stereotypical binding, it is possible to predict target
353 DNA binding sequences solely from amino acid sequences (Gupta et al. 2014). Using this model,
354 we predict the that the common preferred DNA binding sequence for all ZFP-1 homologs
355 examined is 5'-GGGGAA-3' (Figure 4C), based on the sequence conservation of the last two zinc
356 fingers. Given the highly conserved nature of the residues that contribute to sequence-specific
357 binding, we believe that ZFP-1 family proteins function by binding DNA and presumably act as
358 transcription factors.

359

360 ***zfp-1-1* appears to be specifically required for the production of new tegumental cells**

361 If *tsp-2*⁺ cells are tegumental precursors, and *zfp-1* and *zfp-1-1* play a role in the
362 specification of tegumental cells, we would anticipate that loss of *tsp-2*⁺ cells following reduction
363 in *zfp-1* and *zfp-1-1* levels would block the birth of new tegumental cells. Eventually the reduction
364 in tegumental cell birth would result in the reduction in the total number of tegumental cells. To
365 determine if this was the case, we knocked down *zfp-1* or *zfp-1-1* and performed an EdU pulse-
366 chase experiment examining the ability to produce new tegumental cells (Figure 5A). Following
367 *zfp-1* RNAi treatment, we noted a relatively small, but statistically significant, reduction in the
368 percentage of tegumental cells that were EdU⁺ (Figure 5B,C). In contrast to *zfp-1* RNAi treatment,
369 knockdown of *zfp-1-1* led to an almost complete block in the ability of new cells to be added to
370 the tegument (Figure 5B,C). Consistent with these observed reductions in production of new
371 mature tegumental cells, we also noted that RNAi of *zfp-1* or *zfp-1-1* led to 15 and 30 percent

372 reductions in the total density of tegumental cell bodies, respectively (Figure 5B,C). Together
373 these data indicate that both zinc finger proteins are important for tegument specification, but that
374 *zfp-1-1* appears to play a more substantial role in the process.

375 We next sought to determine if loss of *zfp-1* or *zfp-1-1* led to general defects in the ability
376 of parasites to generate non-tegumental lineages. We first monitored the production of new gut
377 cells using the gut-specific marker *cathepsin B*. Like the tegument, the gut is a syncytium, and gut
378 cells appear to be renewed at a relatively high rate (Collins et al. 2013, Collins et al. 2016).
379 Following a 7-day EdU chase period, we noted that *zfp-1-1(RNAi)* parasites generated new gut
380 cells at roughly the same rate as control-treated worms (Figure 5D). Conversely, the rate of new
381 gut cell birth was severely reduced in *zfp-1(RNAi)* worms, suggesting a role for *zfp-1* not just in
382 tegumental differentiation but also in the generation of new gut cells. Given the paucity of cell-
383 type specific markers in schistosomes we next wanted to monitor the general differentiation
384 potential of neoblasts in *zfp-1(RNAi)* and *zfp-1-1(RNAi)* parasites. After a 4-hour EdU pulse >95%
385 of EdU⁺ cells are *nanos2*⁺ (160/166 EdU⁺ nuclei, n=9 male parasites, Figure 3E), therefore, we
386 reasoned that we could monitor the general differentiation potential of neoblasts by examining the
387 amount of EdU-labeled nuclei exiting the *nanos2*⁺ neoblast compartment after a 7-day chase period
388 (Figure 5A). However, since *tsp-2*⁺ cells are the major output of neoblasts (Collins et al. 2016),
389 and neither *zfp-1* nor *zfp-1-1* RNAi treatments completely depleted the *tsp-2*⁺ cell pool, we
390 specifically examined the appearance of EdU⁺*nanos2*⁻*tsp-2*⁻ cells in the parenchyma after a 7 day
391 chase in order to exclude cells related to the tegument lineage. While we noted large numbers of
392 EdU⁺*nanos2*⁻*tsp-2*⁻ cells in both *zfp-1* and *zfp-1-1* RNAi treated parasites, *zfp-1(RNAi)* worms
393 displayed a slight reduction in the total number of EdU⁺*nanos2*⁻*tsp-2*⁻ cells relative to controls

394 (Figure 5E). These data suggest that *zfp-1* may play a more general role in neoblast differentiation,
395 whereas *zfp-1-1* appears to play a more specific role in the production of new tegumental cells.

396 During *in vitro* culture schistosomes use their ventral sucker to attach themselves to the
397 bottom of their cell culture dish (Collins and Collins 2016). In parallel to our observations with
398 *zfp-1-1* in tegumental differentiation, we noted that *zfp-1-1(RNAi)* parasites detached from their
399 culture vessel during RNAi treatment (Figure 5F); a similar phenotype was not observed for either
400 control(RNAi) or *zfp-1(RNAi)* animals (Figure 5F). These data suggest that loss of tegument cell
401 body density following *zfp-1-1 RNAi* may result in gross physical deficits during *in vitro* culture.

402 To explore the effects of *zfp-1-1 RNAi* in more detail, we performed transcriptional
403 profiling of *zfp-1-1(RNAi)* parasites using RNAseq (Figure 5G). As anticipated, RNAi of *zfp-1-1*
404 resulted in reduced expression of transcripts expressed in *tsp-2⁺* cells including *tsp-2*, *meg-1*, and
405 *sm13* (Figure 5G, Supplementary File 4). Consistent with the observed reduction in the total
406 number of tegumental cells following *zfp-1-1(RNAi)* (Figure 5C), we also found that transcripts
407 for the definitive tegumental markers *calpain*, *annexin*, and *npp-5* were significantly down-
408 regulated in *zfp-1-1(RNAi)* parasites (Figure 5H, Supplementary File 4). Importantly, we did not
409 observe significant changes in the expression of genes associated with the schistosome nervous
410 system (e.g., *pc2* (Protasio et al. 2017)) nor in genes associated with the intestine (*cathepsin B*) in
411 *zfp-1-1(RNAi)* parasites (Figure 5H). To further explore the specificity of *zfp-1-1 RNAi* for cells
412 within the tegument lineage, we examined if genes represented by each of our individual
413 expression clusters (Figure 2D) were statistically-enriched among genes down-regulated in *zfp-1-*
414 *1(RNAi)* parasites. If the effects of *zfp-1-1* depletion are largely restricted to the tegumental lineage
415 and not to other tissues, we would anticipate that a majority of genes down-regulated in *zfp-1-*
416 *1(RNAi)* parasites would represent genes expressed in the tegumental lineage. Consistent with this

417 model, we found that clusters of genes with high-levels of TSP-2-enrichment (i.e., 3, 14, 5, and
418 13) were statistically overrepresented among genes down-regulated (\log_2 fold change < -0.5 , padj
419 < 0.05) following *zfp-1-1(RNAi)*. Conversely, clusters with low-levels of *tsp-2* enrichment (i.e.,
420 1, 11, 7, 12, and 15) were statistically underrepresented among genes down-regulated following
421 *zfp-1-1(RNAi)* (Figure 5I). Given these data, and our pulse-chase experiments (Figure 5B-E), the
422 effects of *zfp-1-1* RNAi appear to predominantly affect the maintenance of tegumental cells and
423 their progenitors. Therefore, we suggest that *zfp-1-1* represents a critical and specific regulator of
424 tegumental specification in schistosomes.

425

426 **Discussion**

427 Here, we describe a novel methodology to fluorescently label the schistosome tegument
428 and its associated cell bodies. Using this labeling approach, we defined cell-type specific markers
429 of the tegument, and together with EdU pulse-chase experiments and immunolabeling for TSP-2,
430 we suggest that *tsp-2⁺* cells contribute to the schistosome tegument. Based on our observations
431 we propose a model in which neoblasts specify cells expressing *tsp-2⁺* that migrate through the
432 mesenchyme. As these progenitors approach the tegument, they extend cellular projections that
433 traverse the muscle layers and basement membranes, and ultimately fuse with the outer tegument
434 (Figure 6). Since we find that tegumental cell bodies are subject to physiological cell turnover
435 (Figure 1L,M), and that ablation of tegumental progenitors by *zfp-1* or *zfp-1-1* RNAi results in
436 reduced tegumental cell density (Figure 5B,C), it appears that neoblast-driven tegument renewal
437 is essential for the homeostatic maintenance of tegumental cell number.

438 One outstanding question relates to the molecular composition of cells within the
439 tegumental lineage. Our data suggest that *tsp-2⁺* cells contribute to the tegument, but it is not clear

440 if this property extends to all *tsp-2*-expressing cells. Analysis of genes expressed in FACS-purified
441 TSP-2⁺ cells found that several genes were expressed in subsets of *tsp-2*⁺ cells (Figure 2G, Figure
442 2 - Figure Supplement 2). One possible interpretation of these observations is that these distinct
443 *tsp-2*⁺ populations represent cells at different stages of commitment to a tegumental fate.
444 However, it is possible that certain subsets of *tsp-2*⁺ are destined to generate other non-tegumental
445 lineages. Interestingly, we also observed that a pair of Endophilin B1-encoding genes are
446 expressed in a subset of mature tegumental cells (Figure 2G), opening up the possibility that the
447 tegument is comprised of molecular and functionally distinct cell bodies, despite being a
448 syncytium. Based on the relative distribution of tegument-specific cytoplasmic inclusions, early
449 ultrastructural studies hinted at the possibility that multiple classes of tegumental cell types exist
450 (Morris and Threadgold 1968). Given this possibility, different types of *tsp-2*⁺ cells may give rise
451 to different classes of tegumental cell bodies. Alternatively, a mechanism for tegument cell
452 renewal independent of *tsp-2*⁺ cells may also exist. Detailed studies of these various cell
453 populations using emerging single cell RNA sequencing technology are expected to improve our
454 understanding of this cellular heterogeneity and how it relates to tegument biogenesis.

455 Although both *zfp-1* and *zfp-1-1* are essential for the normal production of tegumental cells,
456 depletion of *zfp-1-1* appears to have a more profound effect on this process (Figure 5B,C). This
457 observation is curious since *tsp-2*⁺ cells are depleted to a similar extent in either *zfp-1(RNAi)* or
458 *zfp-1-1(RNAi)* parasites (Figure 3C,D). However, we did note that *zfp-1-1(RNAi)* resulted in a
459 much greater depletion of cells expressing *sm13* compared to *zfp-1(RNAi)* (Figure 3G,H). One
460 possible explanation of this observation is that *zfp-1* and *zfp-1-1* RNAi treatments have differential
461 effects on cells within the *tsp-2*⁺ compartment. Perhaps *zfp-1* acts in the stem cells to specify early
462 tegumental *tsp-2*⁺ progenitors, whereas *zfp-1-1* acts in early progenitors to control the fate of cells

463 later during the commitment process. Given the effects of *zfp-1-1* on *sm13*⁺ cells, and the location
464 of these cells towards the parasite's surface (Figure 2G), it is possible that *sm13*⁺ cells may -
465 represent a population of late tegumental progenitors. A more detailed examination of the various
466 cells types within the *tsp-2*⁺ compartment is expected to bring clarity to this issue.

467 In addition to the differential effect on *sm13*⁺ cells, we found that *zfp-1-1* RNAi treatment
468 resulted in a gradual detachment of the parasite from their culture vessel (Figure 5F). Parasites rely
469 upon their ventral sucker to attach to blood vessel walls in the host and to the bottom of culture
470 vessels during *in vitro* culture. As the only part of the worm that physically attaches to solid
471 substrate, one might expect the ventral sucker to experience more “wear and tear” than the rest of
472 the organism. Like the rest of the worm, the sucker is covered in tegument. While we cannot say
473 that the detachment phenotype is a direct result of the disruption of tegument maintenance, an
474 attractive hypothesis is that the gross effects of loss of tegument cell renewal are first experienced
475 by the sucker in the form of the inability to attach to substrate. Indeed, this hypothesis is supported
476 by the observation that the effects of *zfp-1-1(RNAi)* are largely limited to tegumental cell
477 populations (Figure 5H-I). Future studies exploring the function of *zfp-1-1* in the context of host
478 infection could provide important insights into the role for tegumental renewal in parasite survival
479 *in vivo*.

480 Our data highlight fundamental similarities in the cellular organization of epidermal
481 lineages between schistosomes and the free-living planarian flatworms. Unlike schistosomes, free-
482 living flatworms (e.g., planarians) possess a simple epidermis comprised of a single layer of
483 epithelial cells that rests upon a basement membrane and several layers of muscles (Hyman 1951,
484 Tyler and Tyler 1997, Tyler and Hooge 2004). Counter to the epidermal maintenance strategies
485 of other long-lived metazoa (e.g., cnidarians (Buzgariu et al. 2015) and mammals (Watt 2001)),

486 where resident stem cells support the renewal of worn out or damaged epithelial cells, the planarian
487 epidermis is unique as it is completely devoid of proliferative cells (Newmark and Sanchez
488 Alvarado 2000). To fulfill a constant demand for new epidermal cells, neoblasts in planarians
489 specify large numbers of post-mitotic epidermal progenitor cells (Newmark and Sanchez Alvarado
490 2000, Eisenhoffer et al. 2008, van Wolfswinkel et al. 2014). In many ways, these epidermal
491 progenitors are similar to *tsp-2*⁺ tegumental progenitors: they appear to be the primary output of
492 neoblasts, they are rapidly lost following neoblast ablation, and they express a variety of species-
493 specific factors. Furthermore, like schistosomes, these progenitors migrate through the
494 mesenchyme, traverse the muscles and basement membrane, and incorporate into the existing
495 epithelium (Newmark and Sanchez Alvarado 2000). Thus, the cellular organization of epidermal
496 maintenance lineages in planarians and schistosomes appears to be quite similar despite resulting
497 in two very different tissues (epidermis vs. tegument).

498 In addition to the similarities in their cellular organization, our data, together with previous
499 studies of planarians (Wagner et al. 2012, van Wolfswinkel et al. 2014), suggest that flatworm
500 epidermal lineages also rely on members of the *zfp-1* family of flatworm-specific transcriptional
501 regulators. Despite the apparent conserved function of these regulators, we do note some
502 differences in the function of *zfp-1* family proteins in planarians and schistosomes. The planarian
503 and schistosome *zfp-1* genes are both expressed in neoblasts, and based on sequence similarity
504 they appear to be orthologous (Figure 4B). However, the planarian protein is specifically required
505 for the maintenance of the epidermal lineage, whereas the schistosome protein appears to be
506 essential for both tegumental and non-tegumental lineages (Figure 5D). Thus, it would appear the
507 schistosome *zfp-1* homolog plays a more general role in cellular differentiation. These
508 observations, however, do not rule out possibility that the schistosome *zfp-1* protein is directly

509 responsible for specifying tegument fates. Indeed, loss of the non-tegumental lineages following
510 *zfp-1* RNAi could represent a compensatory mechanism by the neoblasts to fulfill a high demand
511 for new tegumental cells. Although a specific role for *zfp-1* cannot be demonstrated at this time,
512 the schistosome *zfp-1-1* appears to have a specific role in tegumental fates. Like *zfp-1*, the
513 schistosome *zfp-1-1* has a related homolog in planarians (Figure 4B). While this planarian
514 homolog has not been characterized, recent single cell transcriptional analyses suggest that the
515 expression of this gene is enriched in the epidermal lineage (Wurtzel et al. 2015). Clearly, more
516 detailed studies of these zinc finger proteins, and their roles in epidermal development, in both
517 free-living and parasitic flatworms are essential to determine the significance of these
518 observations.

519 Given these apparent similarities between planarians and schistosomes, and a wealth of
520 evidence indicating that the Neodermata are descendants of free-living flatworms (Ehlers 1985,
521 Egger et al. 2015, Laumer et al. 2015), it is possible that the evolution of the tegument, and
522 perhaps even the emergence of parasitism, has its roots in the epidermal biogenesis programs of
523 the free-living ancestors to modern day Neodermata. By modulating the basic cellular behaviors
524 of epidermal progenitor cells during the course of evolution, perhaps there was a shift from
525 migratory epidermal progenitors that intercalate into the multi-cellular epithelium to fusogenic
526 progenitor cells that give rise to the syncytial tegument. Given this model, we suspect that our
527 observations of neoblast-driven tegument biogenesis in schistosomes are likely to extend to all
528 members of the Neodermata. Therefore, further study of tegumental development is expected to
529 provide clues relevant for understanding the evolutionary forces that gave rise to parasitism in
530 flatworms. Furthermore, since the tegument is critical to parasite biology, understanding the

531 tegument lineage, and the molecular targets of *zfp-1* homologues, in diverse flatworms could
532 suggest novel therapies to blunt tegument development in this important group of parasites.
533

534 **Acknowledgments**

535 We thank Megan McConathy for comments on the manuscript. Mice and *B. glabrata* snails were
536 provided by the NIAID Schistosomiasis Resource Center of the Biomedical Research Institute
537 (Rockville, MD) through NIH-NIAID Contract HHSN272201000005I for distribution through
538 BEI Resources. NVG is an investigator of the Howard Hughes Medical Institute. The authors
539 declare no competing interests.

540
541
542

543 **Figure/Table Legends**

544

545 **Figure 1. *tsp-2*⁺ neoblast progeny cells fuse with the tegumental syncytium in adult**

546 **schistosomes**

547 (A) Cartoon depicting anatomy of the tegument and fluorescent dextran labeling. (B-D)

548 Transverse planes through various levels of the tegument as indicated in (A). Phalloidin labels F

549 actin-rich (B) tegumental spines and pores and (C,D) muscle fibers; fluorescent dextran labels

550 the tegument, cytoplasmic projections, and tegumental cell bodies. (E-F) Side view of dextran-

551 labeled tegument depicting cytoplasmic projections extending from the cell bodies to the surface

552 of the tegument and (F) intercalating between phalloidin-labeled muscle fibers. (G-H) FISH

553 experiments demonstrating the localization of (G) *calp* expression (n= 222 cells from 3 adult

554 male parasites) or (H) *tsp-2* expression relative to the dextran-labeled tegumental cells (n=233

555 cells from 3 adult male parasites). Insets show a Venn diagram illustrating the relative overlap of

556 cell populations. (I) Double FISH experiment demonstrating the localization of *tsp-2* expression

557 relative to *calp* expression (n= 275 cells from 3 adult male parasites). (J) Immunofluorescence in

558 conjunction with FISH demonstrating that TSP-2 protein is found in both *tsp-2*-expressing cells

559 and in the cells expressing a mixture of tegument markers (“Tegument”). (K) Image of a rare *tsp-*

560 *2* mRNA expressing tegumental cell that is also TSP-2 protein positive. (L) EdU pulse-chase

561 experiment examining the kinetics of EdU incorporation into *tsp-2*⁺ cells and definitive

562 tegumental cells. We find that EdU is incorporated into *tsp-2*⁺ cells prior to incorporation into

563 cells expressing tegumental markers, consistent with short lived *tsp-2*-expressing progenitors

564 going on to become mature tegumental cells (n= ~130 cells per animal from 6 adult male

565 parasites per time point). (M) Quantification of EdU incorporation in *tsp-2*⁺ and tegumental
566 cells. Error bars represent 95% confidence intervals. Scale bars: 10µm.

567 **Figure 2. FACS purification and transcriptional profiling identifies molecules expressed in**
568 **neoblasts and cells associated with the tegumental lineage**

569 (A) Cartoon depicting FACS purification strategy. (B) FACS plots showing various cell
570 populations in control and following gamma-irradiation. Percentages represent fraction of the
571 number of cells in the boxed region over the total number of live cells. (C) Confocal
572 micrographs of the sorted cell populations labeled with Hoechst and an anti-TSP-2 antibody. (D)
573 Heatmap showing clustering analysis of genes expressed in the indicated cell populations. Inset
574 shows TSP-2 enriched clusters. (E) Heatmap showing the relative expression of individual genes
575 in each cell population. These genes are organized by cluster. (F) Cartoon depicting the
576 approximate regions imaged in panel G. (G) Maximum intensity projection of z-stacks acquired
577 either at superficial levels (“Surface”) or deeper in the parasite tissue (“Parenchyma”). The gene
578 expression cluster of each gene examined is listed on the right. Scale bars: 10µm.

579 **Figure 3. An RNAi screen identifies *zfp-1* and *zfp-1-1* as genes required for the production**
580 **of *tsp-2*⁺ cells**

581 (A) Cartoon depicting the RNAi screening strategy used to identify regulators of tegument
582 progenitor specification. Candidate genes were knocked-down using RNAi, worms were pulsed
583 with EdU for 4 hours and then fixed. Neoblasts and tegument progenitor cells were observed
584 using EdU detection and *tsp-2* RNA FISH, respectively. (B) Results of control RNAi
585 experiments. Negative control RNAi preserves *tsp-2* cells and neoblasts whereas *h2b* RNAi
586 results in a loss of neoblasts and *tsp-2* cells. *brca1*, *bard*, *fgfr1/4*, and *p53* RNAi results in a

587 partial depletion of neoblasts and a proportional decrease in *tsp-2*⁺ cells. Representative
588 maximum intensity confocal projections are shown. Numbers represent the fraction of parasites
589 displaying the observed phenotype. (C) Maximum intensity projection showing *tsp-2* expression
590 and EdU incorporation in *zfp-1(RNAi)* or *zfp-1-1(RNAi)* parasites. (D) Quantification of the
591 number of *tsp-2*⁺ cells per mm of worm. Control(RNAi) n=17, *zfp-1(RNAi)* n=19, *zfp-1-1(RNAi)*
592 n= 15. (E) Maximum intensity projection showing *nanos2* expression and EdU incorporation in
593 *zfp-1(RNAi)* or *zfp-1-1(RNAi)* parasites. (F) Quantification of the number of EdU⁺ cells per mm
594 worm. Control(RNAi) n=17, *zfp-1(RNAi)* n=19, *zfp-1-1(RNAi)* n= 15. (G) Maximum intensity
595 projection showing *tsp-2* and *sm13* expression in *zfp-1(RNAi)* or *zfp-1-1(RNAi)* parasites. (H)
596 Quantification of the number of *sm13*⁺ cells per mm worm. Control(RNAi) n=17, *zfp-1(RNAi)*
597 n=19, *zfp-1-1(RNAi)* n= 15. (I) WISH showing *zfp-1* expression in adult male worm. (J) Double
598 FISH showing expression of *zfp-1* relative to *nanos2* (a neoblast marker), *zfp-1-1*, and *tsp-2*. (K)
599 WISH showing *zfp-1-1* expression in adult male worm. (L) Double FISH showing expression of
600 *zfp-1-1* relative to *tsp-2*, a mixture tegument-specific markers (tegument), and *nanos2* (a neoblast
601 marker). (M) 3D rendering showing expression of *zfp-1-1* in a subset of *tsp-2*⁺ cells. The dorsal
602 and ventral surfaces of the animal are oriented towards the top and the bottom of the image,
603 respectively, as indicated by the arrows in the first panel. Scale bars: B, C, G, I, K 50μm; E, J, L,
604 M 10μm. Error bars represent 95% confidence intervals, ** p<0.01 (Student's t-test).

605 **Figure 4. ZFP-1 and ZFP-1-1 are flatworm specific zinc finger proteins and are putative**
606 **transcriptional regulators**

607 (A) Multiple protein sequence alignment of the C2H2 domain of several *zfp-1* and *zfp-1-1*
608 homologs. Zinc coordinating residues are shown in black background. Conserved residues
609 contributing to high specificity DNA-binding are highlighted in cyan for the second and third

610 zinc fingers, with the specific DNA base shown below the residue highlighted in yellow. The
611 corresponding positions in the first zinc finger are shown in grey background. The positions
612 determining DNA binding specificity in the first zinc finger (highlighted in grey background)
613 either are not well conserved among these proteins or do not contribute to high specificity of
614 DNA binding. (B) Un-rooted phylogenetic tree of *ZFP-1* and *ZFP-1-1* homologs from multiple
615 species of flatworms. Numbers at the nodes represent bootstrap values. (C) Predicted DNA
616 binding motif of *zfp-1* and *zfp-1-1* of *S. mansoni* by the ZFModels server.

617 **Figure 5. ZFP-1 family proteins are required for the production of new tegumental cells**

618 (A) Cartoon depicting the strategy for fate-mapping by EdU pulse-chase experiments. (B) FISH
619 for *tsp-2* and tegumental markers with EdU detection in *zfp-1(RNAi)* or *zfp-1-1(RNAi)* parasites
620 at day 7 following an EdU pulse. Arrows represent EdU⁺ tegumental cells. (C) (Top)
621 Quantification of the percentage of tegumental cells that are EdU⁺ following a 7-day chase
622 period and (Bottom) tegumental cell density in *zfp-1(RNAi)* or *zfp-1-1(RNAi)* parasites.
623 Control(RNAi) n=12, *zfp-1(RNAi)* n=11, *zfp-1-1(RNAi)* n=8. (D) FISH for *cathepsin B* and EdU
624 detection in *zfp-1(RNAi)* or *zfp-1-1(RNAi)* parasites at day 7 following an EdU pulse. Plot
625 represents the percentage of *cathepsin B*⁺ cells that are EdU⁺. Control(RNAi) n=12, *zfp-1(RNAi)*
626 n=13, *zfp-1-1(RNAi)* n=14. (E) FISH for *nanos2* and *tsp-2* with EdU detection in *zfp-1(RNAi)* or
627 *zfp-1-1(RNAi)* parasites at day 7 following an EdU pulse. Plot represents the number of *tsp-2*
628 EdU⁺ differentiated cells (i.e., *nanos2*⁻ cells) per mm of parasite length. Control(RNAi) n=12,
629 *zfp-1(RNAi)* n=10, *zfp-1-1(RNAi)* n=11. (F) Percentage of the parasites that remain attached to
630 the culture dish at the indicated time point following the first RNAi treatment. n=5 experiments
631 with approximately 10 worms per RNAi treatment in each experiment. (G) Cartoon depicting
632 strategy for examining transcriptional changes following *zfp-1-1* RNAi. (H) Volcano plot

633 showing differentially expressed genes in *zfp-1-1(RNAi)* worms. Red dots represent genes that
634 are down regulated ($-0.5 \log_2$ fold change, $p_{\text{adj}} < 0.05$) in *zfp-1-1(RNAi)* worms. Cyan dots
635 indicate genes known to be expressed in the tegument lineage. Magenta dots indicate genes
636 validated to be expressed in differentiated cells. (I) Plot showing odds-ratio (i.e., the relative
637 over- or under-representation) of genes from gene expression clusters among genes down
638 regulated following *zfp-1-1* RNAi. Blue rectangles depict the odds-ratio from a Fisher's Exact
639 Test, whereas blue lines indicate the 95% confidence intervals. Values of odds-ratio and p-
640 values for Fisher's Exact Test shown to right. No genes from expression clusters 1 or 11 were
641 down-regulated following *zfp-1-1* RNAi, so no odds ratio was calculated. From these data,
642 genes from expression clusters 3, 5, 13 and 14 are over-represented ($p < 0.05$), whereas genes
643 from clusters 1, 7, 9, 11, 12, and 15 appear under-represented. Scale bars: 10 μ m. Error bars in
644 (C-E) represent 95% confidence intervals, error bars in (F) represent standard deviation. * $p <$
645 0.05; ** $p < 0.01$; ns, not significant (Student's t-test).

646 **Figure 6. Model for the specification of new tegumental cells from neoblasts**

647 Neoblasts (magenta cells) expressing *nanos2* and *zfp-1* specify large numbers of *tsp-2*⁺ cells.
648 Some fraction of *tsp-2* cells express *zfp-1-1*. Within this *tsp-2* compartment are cells that extend
649 cytoplasmic projections ultimately fusing with the tegumental syncytium. Loss of *zfp-1* function
650 results in a general differentiation defect (i.e. loss of both tegument progenitors and gut cells)
651 whereas loss of *zfp-1-1* function results in a specific loss of *tsp-2*⁺ cells responsible for
652 replenishing the tegument. In both cases, depletion of *tsp-2*⁺ cells causes a reduction in the total
653 number of tegumental cell bodies.

654

655 **Figure 1-Figure Supplement 1. FISH examining the expression of several candidate**
656 **tegument markers**

657 (A-C) FISH experiments on dextran-labeled worms demonstrating the localization of (A)
658 *annexin* expression (n= 216 cells from 3 adult male parasites), (B) *gtp-4* expression (n= 172 cells
659 from 3 adult male parasites), and (C) *npp-5* expression (n= 199 cells from 3 adult male parasites)
660 relative to dextran-labeled tegumental cells. (D-F) Double FISH experiments demonstrating the
661 localization of *tsp-2* expression relative to (D) *npp-5* expression (n= 492 cells from 3 adult male
662 parasites), (E) *annexin* expression (237 cells from 3 adult male parasites), and (F) *gtp-4*
663 expression (n= 255 cells from 3 adult male parasites). (G) Double FISH experiment
664 demonstrating the localization of *tsp-2* expression relative to *sm13* expression (n= 240 cells from
665 3 adult male parasites). (H) FISH experiment on dextran-labeled worms demonstrating the
666 localization of *sm13* expression relative to dextran-labeled tegumental cells (n= 372 cells from 2
667 adult male parasites). (I-L) Double FISH experiments demonstrating the localization of (I) *calp*
668 expression (n= 291 cells from 3 adult male parasites), (J) *annexin* expression (n= 287 cells from
669 3 adult male parasites), (K) *gtp-4* expression (n= 328 cells from 3 adult male parasites), and (L)
670 *npp-5* expression (n= 269 cells from 3 adult male parasites) relative to *sm13* expression. Insets
671 show a Venn diagram illustrating the relative overlap of cell populations with white representing
672 co-expression. All images were taken at the level of the tegument. Scale bars: 10µm.

673 **Figure 1-Figure Supplement 2. Examination of TSP-2 protein localization**

674 (A) Western blot showing depletion of *TSP-2* protein levels following *tsp-2* RNAi. (B) Cartoon
675 depicting dextran and *TSP-2* labeling of the tegument. (C) Transverse image at the level
676 indicated in (B) demonstrating the specificity of surface labeling of the parasite using anti-*TSP-2*

677 antibody. (D) Double FISH experiment with immunofluorescence demonstrating that *TSP-2*
678 protein is found in both *tsp-2* mRNA⁺ cells as well as in mature tegumental cells. (E) FISH
679 experiment in conjunction with dextran-labeling and immunofluorescence demonstrating that
680 *TSP-2* protein is found in both *tsp-2* mRNA⁺ cells as well as in mature tegumental cells. Scale
681 bars: 10μm.

682 **Figure 2-Figure Supplement 1. Microscopic imaging of sorted “TSP-2 Intermediate” cells**

683 Confocal images of sorted TSP-2 Intermediate cells. Arrows in the inset show cells with no TSP-
684 2 labeling (red arrows), cells with pieces of TSP-2⁺ debris attached to them (yellow arrows), and
685 acellular debris (orange arrows). Scale bar: 10μm.

686 **Figure 2-Figure Supplement 2. Examination of the expression of genes expressed in TSP-2-
687 enriched clusters**

688 FISH for *tsp-2*, a mixture of tegumental makers (Tegument), and panel of 15 genes from various
689 clusters of gene expression (indicated at right of the image). Relative expression levels of each
690 gene in IR Rest, Neoblasts, and TSP-2⁺ cells are indicated in the heatmap to the right,
691 respectively. Images are maximum intensity projections at either the level of the surface (left) or
692 in the parenchyma (right). See Figure 2F for definition of “surface” and “parenchyma”. Scale
693 bars: 10μm.

694 **Figure 2-Figure Supplement 3. Graphical summary of genes expressed in TSP-2-enriched
695 clusters**

696 A graphical summary indicating where in the tegumental lineage genes are expressed. An
697 asterisk next to a gene name indicates that the gene is only expressed in a subset of the

698 population. A superscript “O” next to a gene name indicates that the gene is also expressed in
699 cells not in the proposed tegument lineage.

700 **Figure 3-Figure Supplement 1. RNAi screen of candidate tegument biogenesis regulators**

701 Results of knocking down candidate transcripts that are dispensable for normal neoblast function
702 and *tsp-2*⁺ cell production. Representative maximum intensity confocal projections are shown.
703 Numbers represent the fraction of parasites displaying the observed phenotype. Scale bars: 50µm

704 **Figure 3-Figure Supplement 2. Quantification of gene expression in *zfp-1(RNAi)* and *zfp-1-1(RNAi)* parasites**

706 Quantitative real time PCR analysis of the effects of *zfp-1* and *zfp-1-1* RNAi on the expression of
707 (A) *zfp-1*, (B) *zfp-1-1*, (C) *sm13*, and (D) *tsp-2*. Each bar represents the expression of the
708 indicated gene from an individual biological replicate relative to the expression from a control
709 RNAi treatment group. Expression levels of indicated genes were normalized to both
710 Cytochrome C Oxidase (Smp_900000) and Proteasome Subunit Beta Type-4 (Smp_056500). *
711 $p < 0.05$, ** $p < 0.01$ (Student’s t-test).

712 **Figure 3-Figure Supplement 3. Gene expression patterns of *sm13* and *zfp-1-1***

713 Representative double FISH demonstrating the localization of *sm13* expression relative to *zfp-1-1*
714 *l* expression. 1 of 248 *sm13*⁺ cells was *zfp-1-1* positive. Image represents a z-projection. Scale
715 bar: 10µm.

716

717 **Supplementary File 1.** Pairwise comparisons of transcriptional profiles of neoblasts, TSP-2+
718 cells, and IR Rest cells.

719 **Supplementary File 2.** Results of model-based clustering analysis to define genes whose
720 expression is enriched in either neoblasts, TSP-2+ cells, or IR Rest cells.

721 **Supplementary File 3.** Table of candidate tegument-associated genes, their abbreviations, their
722 gene expression cluster, and their expression pattern.

723 **Supplementary File 4.** Pairwise comparisons of transcriptional profiles of control(RNAi)
724 parasites versus *zfp-1-1*(RNAi) parasites.

725 **Supplementary File 5.** Table of gene names, abbreviations, and oligonucleotides sequences
726 from this study.

727 **Supplementary File 6.** Table of results from Fisher's exact test to define how *zfp-1-1* RNAi
728 treatment affects genes expressed in various gene expression clusters.

729 **Supplementary File 7.** FASTA formatted file with various flatworm ZFP-1 family protein
730 sequences that were used for generating protein alignments and phylogenetic trees.

731 **Movie 1.** Movie depicting the elaborate interconnected network of the parasite's tegument and
732 the attached tegumental cell bodies.

733 **Movie 2.** Movie depicting the localization of TSP-2 protein relative to the tegument and *tsp-2*
734 expressing cells.

735

736

737

738 **Materials and Methods**

739 **Parasite acquisition and culture**

740 Adult *S. mansoni* (6–7 weeks post-infection) were obtained from infected female mice by
741 hepatic portal vein perfusion with 37°C DMEM (Sigma-Aldrich, St. Louis, MO) plus 10%
742 Serum (either Fetal Calf Serum or Horse Serum) and heparin. Parasites were cultured as
743 previously described (Collins et al. 2016). Unless otherwise noted, all experiments were
744 performed with male parasites.

745 **RNA interference**

746 For *tsp-2* RNAi experiments, 10 freshly perfused male parasites (either as single worms
747 or paired with females) were treated with 20 µg/ml dsRNA for 3 days in Basch Media 169.
748 dsRNA was generated by *in vitro* transcription and was replaced every day. On the 3rd day, the
749 worms were given fresh media. Thereafter, every 3 days the worms received fresh media and 20
750 µg/ml dsRNA for a total of 28 days and then the parasites were fixed as previously described
751 (Collins et al. 2013). For the candidate RNAi screen, 10 freshly perfused male parasites (either
752 as single worms or paired with females) were treated with 30 µg/ml dsRNA for 7 days in Basch
753 Media 169. dsRNA was generated by *in vitro* transcription and was replaced every day. On the
754 8th day, the worms were given fresh media. Thereafter, every 4th day the worms received 60
755 µg/ml dsRNA (~24 hours of exposure to dsRNA before the media was changed) for a total of 17
756 days. On day 17, the worms were pulsed with 10 µM EdU for 4 hours before being fixed as
757 previously described (Collins et al. 2013). The candidate screen was performed twice.

758 For EdU pulse-chase RNAi experiments, 10 freshly perfused male parasites (either as
759 single worms or paired with females) were treated with 30 µg/ml dsRNA for 7 days in Basch
760 Media 169. dsRNA was generated by *in vitro* transcription and was replaced every day. On the

761 8th day, the worms were given fresh media. Thereafter, every 4th day the worms received 60
762 µg/ml dsRNA (~24 hours of exposure to dsRNA before the media was changed) for a total of 28
763 days. On day 21, the worms were pulsed with 10 µM EdU for 4 hours after which the media was
764 changed. On day 28, the worms were fixed as previously described (Collins et al. 2013).
765 As a negative control for RNAi experiments, we used a non-specific dsRNA containing two
766 bacterial genes (Collins et al. 2010). cDNAs used for RNAi and in situ hybridization analyses
767 were cloned as previously described (Collins et al. 2010); oligonucleotide primer sequences are
768 listed in Supplementary File 5. Quantitative PCR analyses to examine knockdown efficiency
769 were performed as previously described (Collins et al. 2013, Collins et al. 2016).

770 **Parasite labeling and imaging**

771 Colorimetric and fluorescence in situ hybridization analyses were performed as
772 previously described (Collins et al. 2013, Collins et al. 2016). To strongly label the entire
773 cytoplasm of tegumental cells by FISH, in some instances we pooled probes recognizing the
774 tegument-specific markers *calpain*, *gtp-4*, *annexin*, and *npp-5*. For dextran labeling, freshly
775 perfused worms were collected in the bottom of a 15 ml conical tube, all residual media was
776 removed, and 100 µl of 5 mg/ml solution of biotin-TAMRA-dextran (Life Technologies D3312)
777 dissolved in ultrapure water was added to ~50 parasites. These worms were constantly agitated
778 by gentle vortexing for 3-4 minutes, and then doused with 10 ml of fixative solution (4%
779 formaldehyde in PBSTx (PBS + 0.3% triton-X100)) to stop the labeling. The fixative solution
780 was removed and replaced with 10 ml of fresh fixative solution to dilute residual dextran. The
781 worms were fixed for 4 hours in the dark with mild agitation. Worms were then washed with 10
782 ml of fresh PBSTx for 10 minutes. Dextran-labeled worms were then labeled with Alexa Fluor
783 488-conjugated phalloidin (Lifetechn A12379) (1:40 dilution in 1% bovine serum albumin in

784 PBSTx) overnight or dehydrated in methanol and processed for in situ hybridization or
785 immunofluorescence. *In vivo* and *in vitro* EdU labeling and detection experiments were
786 performed as previously described (Collins et al. 2013). However, for the 5-week *in vivo* EdU
787 pulse-chase experiments, mice were only exposed to ~30 cercariae to assure the mice would not
788 succumb to schistosome infection prior to the end of the experiment. For immunofluorescence,
789 worms processed for in situ hybridization or dextran labeling were incubated in blocking
790 solution (0.1 M Tris pH 7.5, 0.15 M NaCl and 0.1% Tween-20 with 5% Horse Serum and 0.5%
791 Roche Western Blocking Reagent (King and Newmark 2013)) for 1 hr at room temperature and
792 incubated overnight in affinity purified anti-TSP-2 (Pearson et al. 2012) diluted 1:1000 in
793 blocking solution at 4°C. The following day samples were washed 6x 20 m in PBSTx, incubated
794 overnight in a 1:1000 dilution of AlexaFluor 488 goat anti-rabbit antibody (Thermo Fisher
795 Scientific A11034) in blocking solution, and washed in PBSTx. All fluorescently labeled
796 parasites were counterstained with DAPI (1 µg/ml), cleared in 80% glycerol, and mounted on
797 slides with Vectashield (Vector Laboratories).

798 Confocal imaging of fluorescently labeled samples was performed on either a Zeiss
799 LSM700 or a Nikon A1 Laser Scanning Confocal Microscope. Unless otherwise stated all
800 fluorescence images are taken at the anatomical level of the tegumental cell bodies (see figure
801 1D for approximate location) and represent maximum intensity projections. To perform cell
802 counts, cells were manually counted in maximum intensity projections derived from confocal
803 stacks. We used two types of measurements to normalize cell counts between samples. In cases
804 where we determined the number of cells in a particular region of the parasite (e.g., tegument)
805 we collected confocal stacks and normalized the number of cells by total volume of the stack in
806 µm³. In cases where we determined the total number of labeled foci throughout the entire depth

807 of the parasite (e.g. EdU counts), we collected confocal stacks and normalized the number of
808 cells to the length of the parasite in the imaged region in mm. Brightfield images were acquired
809 on a Zeiss AxioZoom V16 equipped with a transmitted light base and a Zeiss AxioCam 105
810 Color camera.

811

812 **Fluorescence Activated Cell Sorting**

813 Freshly perfused worms were either exposed to 100 Gy of Gamma Irradiation on a J.L.
814 Shepard Mark I-30 Cs¹³⁷ source or left alone to serve as controls, then cultured for one week.
815 After one week, males were separated from female worms by incubation in a 0.25% solution of
816 tricaine (Collins et al. 2013). Male worms were amputated to remove the head and testes, and the
817 bodies of the worms were collected. These worm bodies were briefly minced with a razor blade
818 and then suspended in a 0.5% solution of Trypsin/EDTA (Sigma T4174) in PBS. The worms
819 were then triturated for approximately 15 minutes until the solution became turbid and no large
820 pieces of worms were left. The cells were then centrifuged at 500 g for 10 m at 4°C. Next the
821 cells were resuspended in 1 ml of Basch media with 10 µl of RQ1 DNase (Promega M6101) and
822 incubated for 10 minutes at RT. The cells were centrifuged again at 500 g for 10 minutes at 4°C.
823 The cells were resuspended in staining media (0.5% BSA, 2 mM EDTA in PBS) and incubated
824 in anti-TSP-2 polyclonal antibody (1:1000 dilution) for 45 minutes in the dark at 4°C. The cells
825 were centrifuged again at 500 g for 10 minutes at 4°C. The cells were then resuspended in
826 staining media and incubated in Hoechst 33342 (18 µg/ml) (Sigma B2261) and goat anti-rabbit
827 AF488 (Thermo Fisher Scientific A11034) (1:1000 dilution) for 1 hour at RT in the dark. The
828 cells were centrifuged once again at 500 g for 10 minutes at 4°C. The cells were then
829 resuspended in staining media containing Hoechst 33342 (18 µg/ml) and propidium iodide (1

830 $\mu\text{g/ml}$) (Sigma-Aldrich P4170) and then filtered through a 40 μm cell strainer. Filtered cells were
831 then sorted on a FACSAria Fusion (BD Biosystems) with a 100 μm nozzle either into staining
832 media for confocal imaging or directly into Trizol LS (Thermo Fisher Scientific 10296-010) for
833 RNAseq experiments. For all FACS experiments, a Hoechst threshold was applied to exclude
834 debris and improve the efficiency of sorting.

835

836 **Transcriptional profiling by RNA sequencing**

837 RNA was extracted from purified cells (>40000 “Neoblast”, >4000 “TSP-2⁺”, and 80000
838 “IR Rest” cells per biological replicate) collected from three independent FACS runs using
839 Trizol LS (Thermo Fisher Scientific 10296-010). Libraries for RNAseq analysis were generated
840 using the SMART-seq2 kit (Clontech) and reads obtained by Illumina sequencing. The total
841 number of reads per gene was determined by mapping the reads to the *S. mansoni* genome using
842 STAR (version 020201) (Dobin et al. 2013). *S. mansoni* genome sequence and GTF files used
843 for mapping were acquired from Wormbase Parasite (Howe et al. 2016). Pairwise comparisons
844 of differential gene expression were performed with DESeq2 (version 1.12.2) (Love et al. 2014).
845 To determine which genes showed the highest level of enrichment in the various cell populations
846 we also performed Model Based clustering using the MBCluster.seq package in R (Si et al.
847 2014). This clustering analysis was only performed on genes that had more than 200 total reads
848 from the Neoblast, TSP-2⁺, and IR-REST cell populations. Raw data for RNAseq of FACS
849 sorted cells are available at NCBI under the accession numbers as follows: Neoblasts
850 (ERS1987942, ERS1987945, ERS1987957), TSP-2 HI (ERS1987946, ERS1987958,
851 ERS1987961) and IR Rest (ERS1987948, ERS1987962, ERS1987958). For RNAseq analysis of
852 *zfp-1-1(RNAi)* parasites, Illumina reads for three biological replicates were mapped to the

853 schistosome genome using STAR and differential gene expression changes were measured using
854 DESeq2. The statistical enrichment of the various clusters of genes that were down-regulated
855 following *zfp-1-1(RNAi)* ($\log_2 < -0.5$, $\text{padj} < 0.05$) was measured using a Fisher's exact test in R.
856 Data used for the analysis is provided in Supplementary File 6. RNAseq datasets for the *zfp-1-*
857 *1(RNAi)* experiments are available at NCBI through the accession number GSE106693.

858

859 **Western blotting to detect TSP-2**

860 To generate protein lysates, RNAi treated male parasites were separated with 0.5%
861 tricaine, their heads and testes were amputated, the remaining somatic tissue was homogenized
862 in 100 μl of sample buffer (236 mM Tris pH 6.7, 128 mM H_3PO_4 , 4% SDS, 20% Glycerol, 10
863 mM DTT, and protease inhibitors (Roche cOmplete, Mini, EDTA-free)). Homogenized samples
864 were incubated at 42°C for 45 min and alkylated with N-ethylmaleimide for 40 minutes at 37°C.
865 Protein concentrations were determined by BCA assays, 40 μg of lysate was separated by SDS
866 PAGE, proteins were transferred to nitrocellulose membranes, membranes were blocked in Li-
867 Cor Odyssey Blocking Buffer, incubated in rabbit anti-TSP-2 (1:5000) and mouse anti-Actin
868 (0.25 $\mu\text{g}/\text{ml}$, Monoclonal JLA20, Developmental Studies Hybridoma Bank), washed in TBST,
869 and incubated in secondary antibodies (1:10,000 goat anti-rabbit IRDye 680 RD, 1:15,000 goat
870 anti-mouse IgM IRDye 800CW, Li-Cor). Blots were imaged using a Li-Cor Odyssey Infrared
871 Imager.

872

873 **Protein alignments and Phylogenetic Tree**

874 To estimate the evolutionary relationship between the various flatworm ZFP-1 family
875 members, protein sequences of these family members were aligned using Guidance

876 (<http://guidance.tau.ac.il>) (settings: MSA Algorithm = MAFFT; --maxiterate 1000 --genafpair;
877 number of alternative guide-trees: 100). Columns in the sequence alignment with a confidence
878 score below 0.050 were removed and a tree was generated using RAxML (version 8.0.0)
879 (options -T 4 -f a -p 11111 -x 1111 -# 1000 -m PROTGAMMAAUTO). Sequences used for
880 phylogenetic analysis were recovered from Wormbase Parasite (Howe et al. 2016)
881 (<https://parasite.wormbase.org>), Planmine (Brandl et al. 2016) (<http://planmine.mpi-cbg.de>), the
882 *Gyrodactylus salaris* genome database (<http://invitro.titan.uio.no/gyrodactylus/index.html>)
883 (Hahn et al. 2014), and the *Macrostomum lignano* genome initiative database (Simanov et al.
884 2012) (<http://www.macgenome.org>). A FASTA formatted file can be found in Supplementary
885 File 7. *S. mansoni* ZFP-1 and ZFP-1-1 DNA binding motifs were predicted using the ZFModels
886 web server at <http://stormo.wustl.edu/ZFModels/> (Gupta et al. 2014).

887

888

889

890 **References**

- 891 Brandl, H., H. Moon, M. Vila-Farre, S. Y. Liu, I. Henry and J. C. Rink (2016). "PlanMine--a
892 mineable resource of planarian biology and biodiversity." Nucleic Acids Res **44**(D1): D764-773.
893
- 894 Braschi, S. and R. A. Wilson (2006). "Proteins exposed at the adult schistosome surface revealed
895 by biotinylation." Mol Cell Proteomics **5**(2): 347-356.
896
- 897 Brayer, K. J. and D. J. Segal (2008). "Keep your fingers off my DNA: protein-protein
898 interactions mediated by C2H2 zinc finger domains." Cell Biochem Biophys **50**(3): 111-131.
899
- 900 Buzgariu, W., S. Al Haddad, S. Tomczyk, Y. Wenger and B. Galliot (2015). "Multi-functionality
901 and plasticity characterize epithelial cells in Hydra." Tissue Barriers **3**(4): e1068908.
902
- 903 Charrin, S., S. Jouannet, C. Boucheix and E. Rubinstein (2014). "Tetraspanins at a glance." J
904 Cell Sci **127**(Pt 17): 3641-3648.
905
- 906 Collins, J. J., III, X. Hou, E. V. Romanova, B. G. Lambrus, C. M. Miller, A. Saberi, J. V.
907 Sweedler and P. A. Newmark (2010). "Genome-Wide Analyses Reveal a Role for Peptide
908 Hormones in Planarian Germline Development." PLoS Biol **8**(10): e1000509.
909
- 910 Collins, J. J., III, B. Wang, B. G. Lambrus, M. E. Tharp, H. Iyer and P. A. Newmark (2013).
911 "Adult somatic stem cells in the human parasite *Schistosoma mansoni*." Nature **494**(7438): 476-
912 479.
913
- 914 Collins, J. J., G. R. Wendt, H. Iyer and P. A. Newmark (2016). "Stem cell progeny contribute to
915 the schistosome host-parasite interface." Elife **5**.
916
- 917 Collins, J. N. and J. J. Collins, 3rd (2016). "Tissue Degeneration following Loss of *Schistosoma*
918 *mansoni* *cbp1* Is Associated with Increased Stem Cell Proliferation and Parasite Death In Vivo." PLoS Pathog **12**(11): e1005963.
919
- 920
- 921 Dobin, A., C. A. Davis, F. Schlesinger, J. Drenkow, C. Zaleski, S. Jha, P. Batut, M. Chaisson and
922 T. R. Gingeras (2013). "STAR: ultrafast universal RNA-seq aligner." Bioinformatics **29**(1): 15-
923 21.
924
- 925 Egger, B., F. Lapraz, B. Tomiczek, S. Muller, C. Dessimoz, J. Girstmair, N. Skunca, K. A.
926 Rawlinson, C. B. Cameron, E. Beli, M. A. Todaro, M. Gammoudi, C. Norena and M. J. Telford
927 (2015). "A transcriptomic-phylogenomic analysis of the evolutionary relationships of
928 flatworms." Curr Biol **25**(10): 1347-1353.
929
- 930 Ehlers, U. (1985). Das Phylogenetische System der Plathelminthes. Stuttgart.
931
- 932 Eisenhoffer, G. T., H. Kang and A. Sánchez Alvarado (2008). "Molecular analysis of stem cells
933 and their descendants during cell turnover and regeneration in the planarian *Schmidtea*
934 *mediterranea*." Cell Stem Cell **3**(3): 327-339.

935
936 Gupta, A., R. G. Christensen, H. A. Bell, M. Goodwin, R. Y. Patel, M. Pandey, M. S. Enuameh,
937 A. L. Rayla, C. Zhu, S. Thibodeau-Beganny, M. H. Brodsky, J. K. Joung, S. A. Wolfe and G. D.
938 Stormo (2014). "An improved predictive recognition model for Cys(2)-His(2) zinc finger
939 proteins." Nucleic Acids Res **42**(8): 4800-4812.
940
941 Hahn, C., B. Fromm and L. Bachmann (2014). "Comparative genomics of flatworms
942 (platyhelminthes) reveals shared genomic features of ecto- and endoparasitic neodermata."
943 Genome Biol Evol **6**(5): 1105-1117.
944
945 Hall, T. M. (2005). "Multiple modes of RNA recognition by zinc finger proteins." Curr Opin
946 Struct Biol **15**(3): 367-373.
947
948 Halton, D. W. (1997). "Nutritional adaptations to parasitism within the platyhelminthes." Int J
949 Parasitol **27**(6): 693-704.
950
951 Harris, A. R., R. J. Russell and A. D. Charters (1984). "A review of schistosomiasis in
952 immigrants in Western Australia, demonstrating the unusual longevity of *Schistosoma mansoni*."
953 Trans R Soc Trop Med Hyg **78**(3): 385-388.
954
955 Hayashi, T., M. Asami, S. Higuchi, N. Shibata and K. Agata (2006). "Isolation of planarian X-
956 ray-sensitive stem cells by fluorescence-activated cell sorting." Dev Growth Differ **48**(6): 371-
957 380.
958
959 Hockley, D. J. (1973). "Ultrastructure of the tegument of *Schistosoma*." Adv Parasitol **11**(0):
960 233-305.
961
962 Hockley, D. J. and D. J. McLaren (1973). "*Schistosoma mansoni*: changes in the outer
963 membrane of the tegument during development from cercaria to adult worm." Int J Parasitol
964 **3**(1): 13-25.
965
966 Hornstein, L., G. Lederer, J. Schechter, Z. Greenberg, R. Boem, B. Bilguray, L. Giladi and J.
967 Hamburger (1990). "Persistent *Schistosoma mansoni* infection in Yemeni immigrants to Israel."
968 Isr J Med Sci **26**(7): 386-389.
969
970 Hotez, P. J. and A. Fenwick (2009). "Schistosomiasis in Africa: an emerging tragedy in our new
971 global health decade." PLoS Negl Trop Dis **3**(9): e485.
972
973 Howe, K. L., B. J. Bolt, M. Shafie, P. Kersey and M. Berriman (2016). "WormBase ParaSite - a
974 comprehensive resource for helminth genomics." Mol Biochem Parasitol.
975
976 Hyman, L. (1951). The Invertebrates: Platyhelminthes and Rhynchocoela The Acoelomate
977 Bilateria. New York, McGraw-Hill Book Company, Inc.
978
979 King, R. S. and P. A. Newmark (2013). "In situ hybridization protocol for enhanced detection of
980 gene expression in the planarian *Schmidtea mediterranea*." BMC Dev Biol **13**: 8.

981
982 Klug, A. (2010). "The discovery of zinc fingers and their applications in gene regulation and
983 genome manipulation." Annu Rev Biochem **79**: 213-231.
984
985 Krishna, S. S., I. Majumdar and N. V. Grishin (2003). "Structural classification of zinc fingers:
986 survey and summary." Nucleic Acids Res **31**(2): 532-550.
987
988 Laumer, C. E., A. Hejnlol and G. Giribet (2015). "Nuclear genomic signals of the
989 'microturbellarian' roots of platyhelminth evolutionary innovation." Elife **4**.
990
991 Littlewood, D. T. J. (2006). The Evolution of Parasitism in Flatworms. Parasitic Flatworms:
992 Molecular Biology, Biochemistry, Immunology, and Physiology. A. G. Maule and N. J. Marks.
993 Oxfordshire, UK, CAB International 1-36.
994 Littlewood, D. T. J. and R. A. Bray (2001). Interrelationships of the Platyhelminthes. London,
995 Taylor & Francis.
996
997 Love, M. I., W. Huber and S. Anders (2014). "Moderated estimation of fold change and
998 dispersion for RNA-seq data with DESeq2." Genome Biol **15**(12): 550.
999
1000 McLaren, D. J. (1980). Schistosoma mansoni: The parasite surface in Relation to Host Immunity.
1001 Letchworth, England, John Wiley & Sons, Ltd.
1002
1003 Morris, G. P. and L. T. Threadgold (1968). "Ultrastructure of the tegument of adult *Schistosoma*
1004 *mansoni*." J Parasitol **54**(1): 15-27.
1005
1006 Newmark, P. A. and A. Sanchez Alvarado (2000). "Bromodeoxyuridine specifically labels the
1007 regenerative stem cells of planarians." Dev Biol **220**(2): 142-153.
1008
1009 Payet, B., G. Chaumentin, M. Boyer, P. Amaranto, C. Lemonon-Meric and F. Lucht (2006).
1010 "Prolonged latent schistosomiasis diagnosed 38 years after infestation in a HIV patient." Scand J
1011 Infect Dis **38**(6-7): 572-575.
1012
1013 Pearson, M. S., D. A. Pickering, H. J. McSorley, J. M. Bethony, L. Tribolet, A. M. Dougall, P. J.
1014 Hotez and A. Loukas (2012). "Enhanced protective efficacy of a chimeric form of the
1015 schistosomiasis vaccine antigen Sm-TSP-2." PLoS Negl Trop Dis **6**(3): e1564.
1016
1017 Protasio, A. V., S. van Dongen, J. Collins, L. Quintais, D. M. Ribeiro, F. Sessler, M. Hunt, G.
1018 Rinaldi, J. J. Collins, A. J. Enright and M. Berriman (2017). "MiR-277/4989 regulate
1019 transcriptional landscape during juvenile to adult transition in the parasitic helminth *Schistosoma*
1020 *mansoni*." PLoS Negl Trop Dis **11**(5): e0005559.
1021
1022 Rofatto, H. K., C. A. Tararam, W. C. Borges, R. A. Wilson, L. C. Leite and L. P. Farias (2009).
1023 "Characterization of phosphodiesterase-5 as a surface protein in the tegument of *Schistosoma*
1024 *mansoni*." Mol Biochem Parasitol **166**(1): 32-41.
1025

1026 Si, Y., P. Liu, P. Li and T. P. Brutnell (2014). "Model-based clustering for RNA-seq data."
1027 Bioinformatics **30**(2): 197-205.
1028

1029 Simanov, D., I. Mellaart-Straver, I. Sormacheva and E. Berezikov (2012). "The Flatworm
1030 *Macrostomum lignano* Is a Powerful Model Organism for Ion Channel and Stem Cell Research."
1031 Stem Cells Int **2012**: 167265.
1032

1033 Skelly, P. J. and C. B. Shoemaker (1996). "Rapid appearance and asymmetric distribution of
1034 glucose transporter SGTP4 at the apical surface of intramammalian-stage *Schistosoma mansoni*."
1035 Proc Natl Acad Sci U S A **93**(8): 3642-3646.
1036

1037 Skelly, P. J. and C. B. Shoemaker (2001). "The *Schistosoma mansoni* host-interactive tegument
1038 forms from vesicle eruptions of a cyton network." Parasitology **122 Pt 1**: 67-73.
1039

1040 Skelly, P. J. and R. A. Wilson (2006). "Making sense of the schistosome surface." Adv Parasitol
1041 **63**: 185-284.
1042

1043 Sotillo, J., M. Pearson, J. Potriquet, L. Becker, D. Pickering, J. Mulvenna and A. Loukas (2016).
1044 "Extracellular vesicles secreted by *Schistosoma mansoni* contain protein vaccine candidates." Int
1045 J Parasitol **46**(1): 1-5.
1046

1047 Tran, M. H., M. S. Pearson, J. M. Bethony, D. J. Smyth, M. K. Jones, M. Duke, T. A. Don, D. P.
1048 McManus, R. Correa-Oliveira and A. Loukas (2006). "Tetraspanins on the surface of
1049 *Schistosoma mansoni* are protective antigens against schistosomiasis." Nat Med **12**(7): 835-840.
1050

1051 Tyler, S. and M. Hooge (2004). "Comparative morphology of the body wall in flatworms
1052 (Platyhelminthes)." Can. J. Zool. **82**: 194-210.
1053

1054 Tyler, S. and M. S. Tyler (1997). "Origin of the epidermis in parasitic platyhelminths." Int J
1055 Parasitol **27**(6): 715-738.
1056

1057 van Balkom, B. W., R. A. van Gestel, J. F. Brouwers, J. Krijgsveld, A. G. Tielens, A. J. Heck
1058 and J. J. van Hellemond (2005). "Mass spectrometric analysis of the *Schistosoma mansoni*
1059 tegumental sub-proteome." J Proteome Res **4**(3): 958-966.
1060

1061 van Wolfswinkel, J. C., D. E. Wagner and P. W. Reddien (2014). "Single-Cell Analysis Reveals
1062 Functionally Distinct Classes within the Planarian Stem Cell Compartment." Cell Stem Cell
1063 **15**(3): 326-339.
1064

1065 Wagner, D. E., J. J. Ho and P. W. Reddien (2012). "Genetic regulators of a pluripotent adult
1066 stem cell system in planarians identified by RNAi and clonal analysis." Cell Stem Cell **10**(3):
1067 299-311.
1068

1069 Watt, F. M. (2001). "Stem cell fate and patterning in mammalian epidermis." Curr Opin Genet
1070 Dev **11**(4): 410-417.
1071

1072 Wilson, R. A. (2012). "Proteomics at the schistosome-mammalian host interface: any prospects
1073 for diagnostics or vaccines?" Parasitology **139**(9): 1178-1194.
1074
1075 Wilson, R. A. and P. E. Barnes (1974). "The tegument of *Schistosoma mansoni*: observations on
1076 the formation, structure and composition of cytoplasmic inclusions in relation to tegument
1077 function." Parasitology **68**(2): 239-258.
1078
1079 Wolfe, S. A., L. Nekludova and C. O. Pabo (2000). "DNA recognition by Cys2His2 zinc finger
1080 proteins." Annu Rev Biophys Biomol Struct **29**: 183-212.
1081
1082 Wurtzel, O., L. E. Cote, A. Poirier, R. Satija, A. Regev and P. W. Reddien (2015). "A Generic
1083 and Cell-Type-Specific Wound Response Precedes Regeneration in Planarians." Dev Cell **35**(5):
1084 632-645.
1085
1086
1087

Figure 1

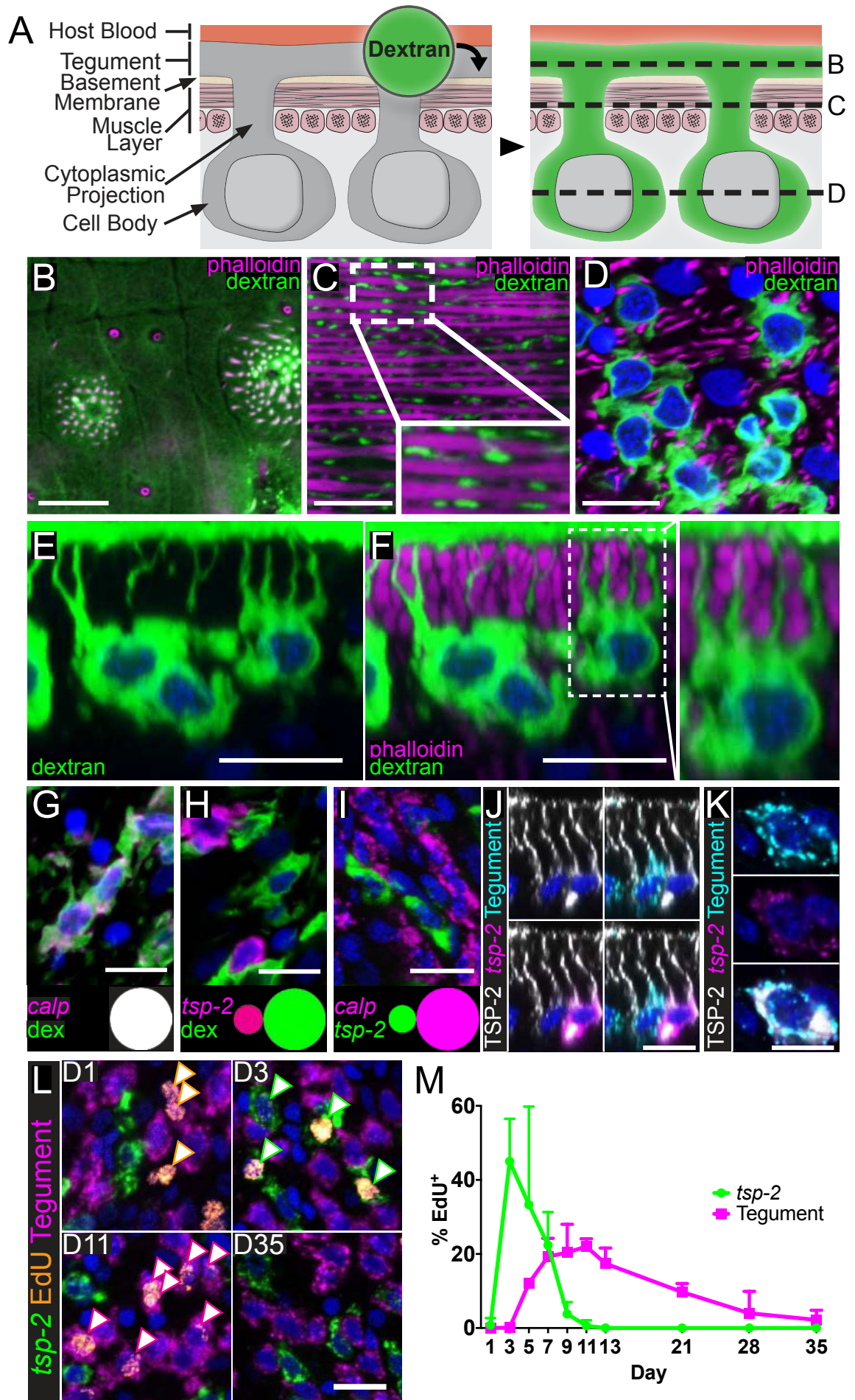


Figure 1-Figure Supplement 1

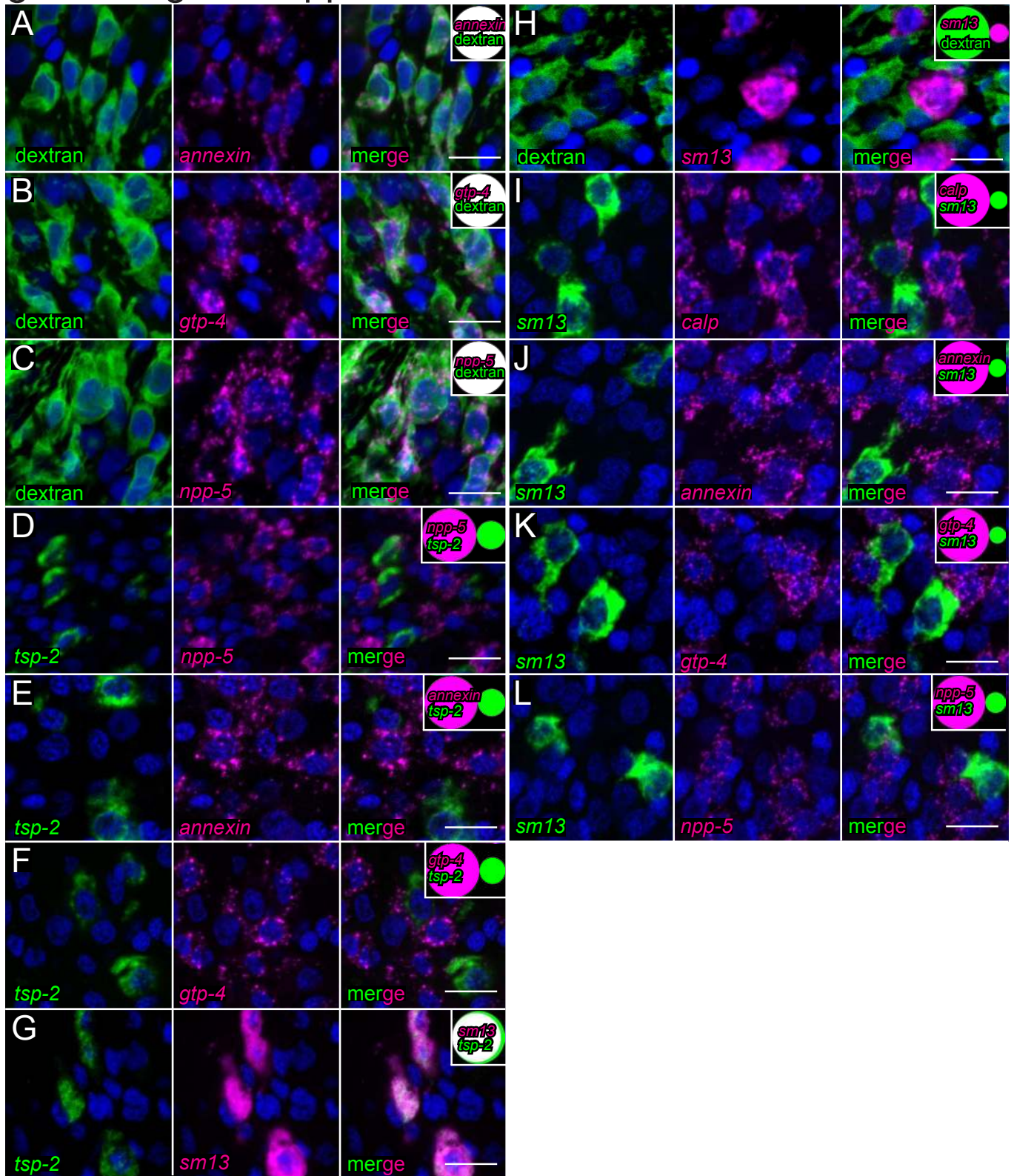
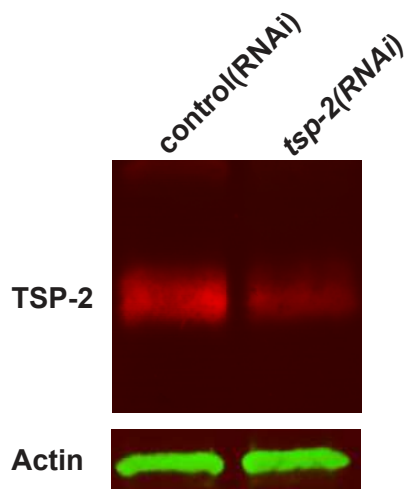
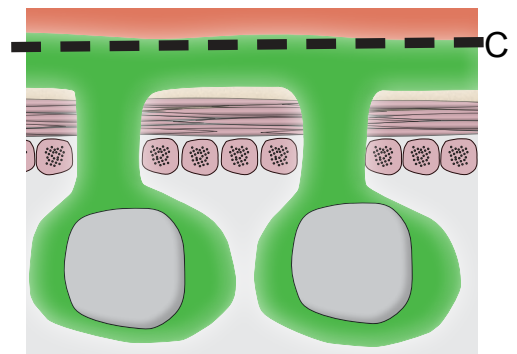


Figure 1-Figure Supplement 2

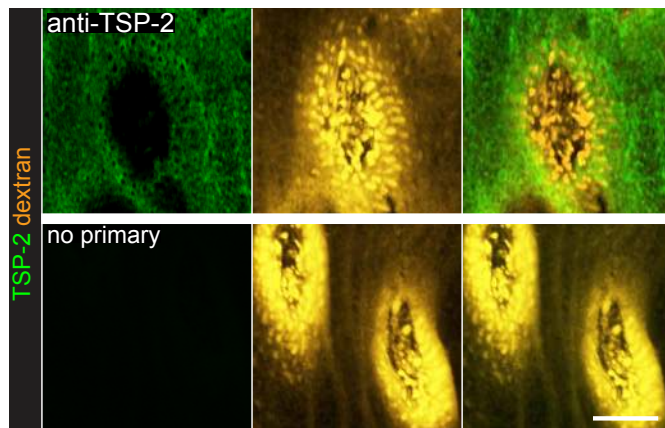
A



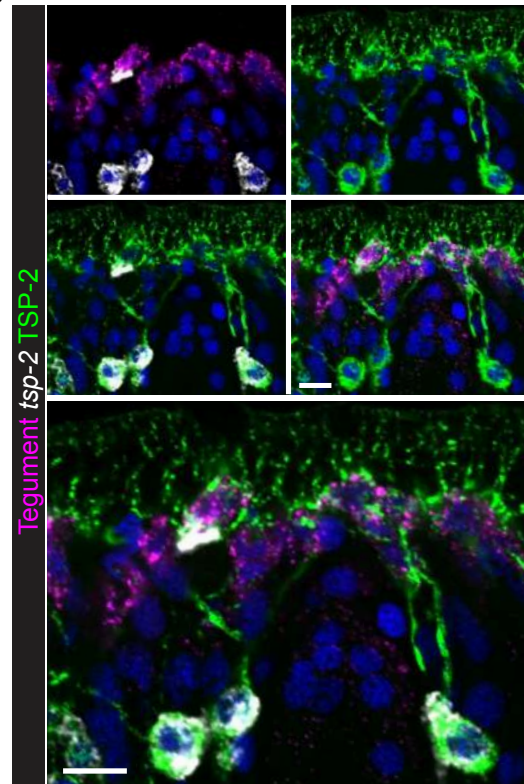
B



C



D



E

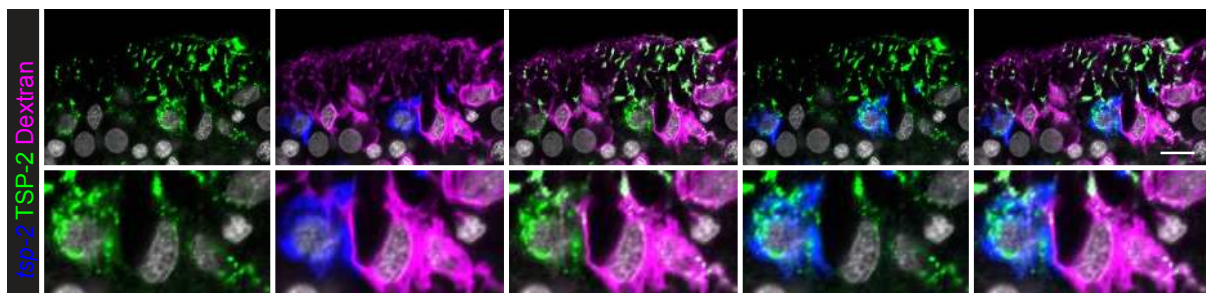


Figure 2

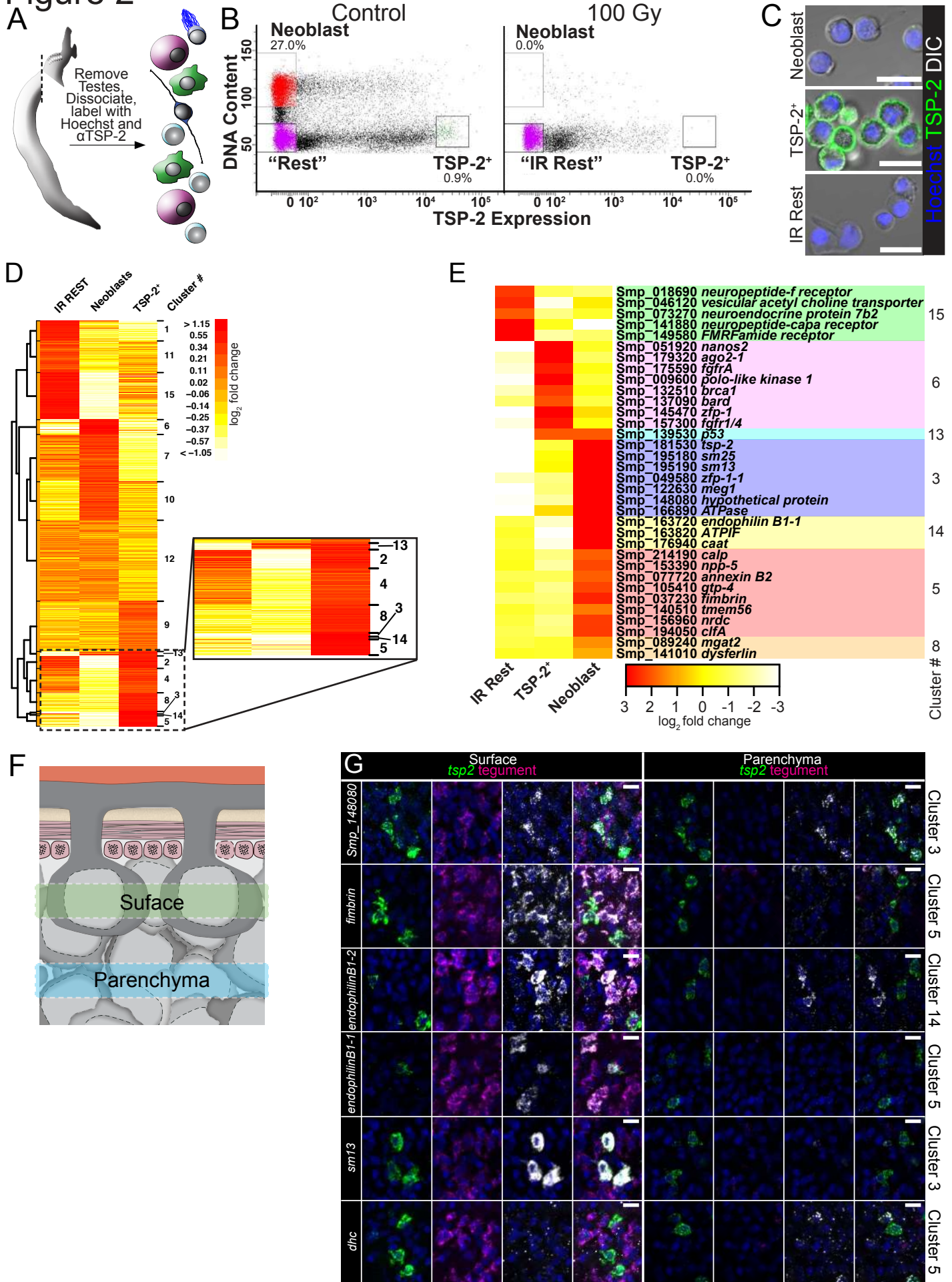


Figure 2-Figure Supplement 1

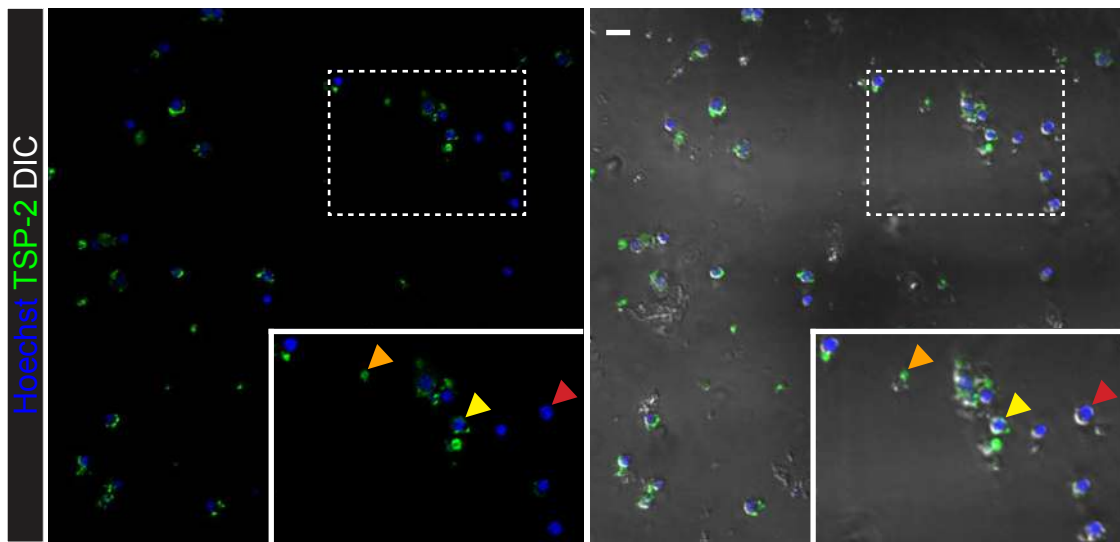
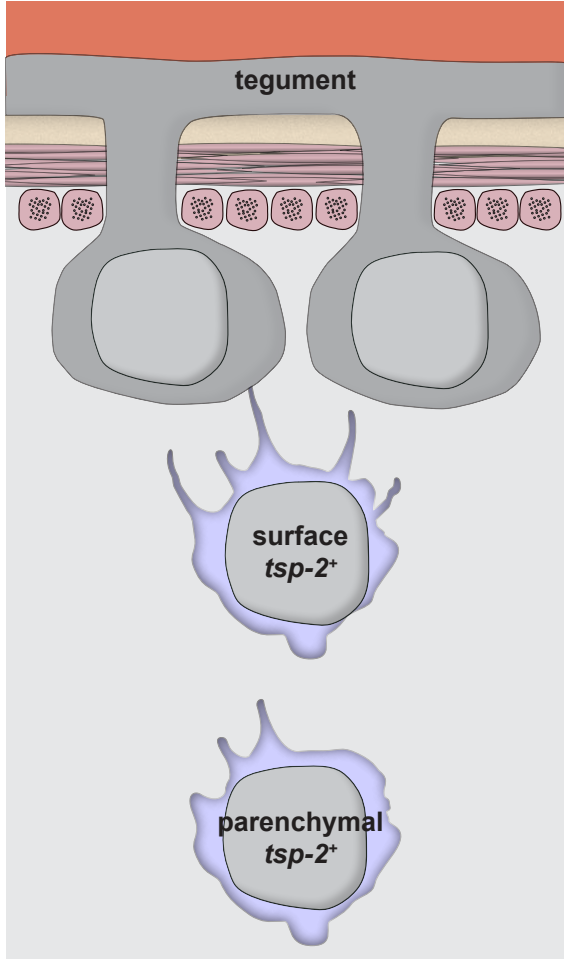


Figure 2-Figure Supplement 3



endophilinB1-2^o*
ATPase nrdc^o
cd59-like^o pla2
mgat2 npp-5
gtp-4 tmem56
annexin b2 calp

fimbrin endophilinB1-1 dysferlin*

pctp

caat

dhc rer1*
zfp-1-1

sm25 sm13
clfA^o

Smp_148080 epsin4 sgms1 z-protein

Figure 3

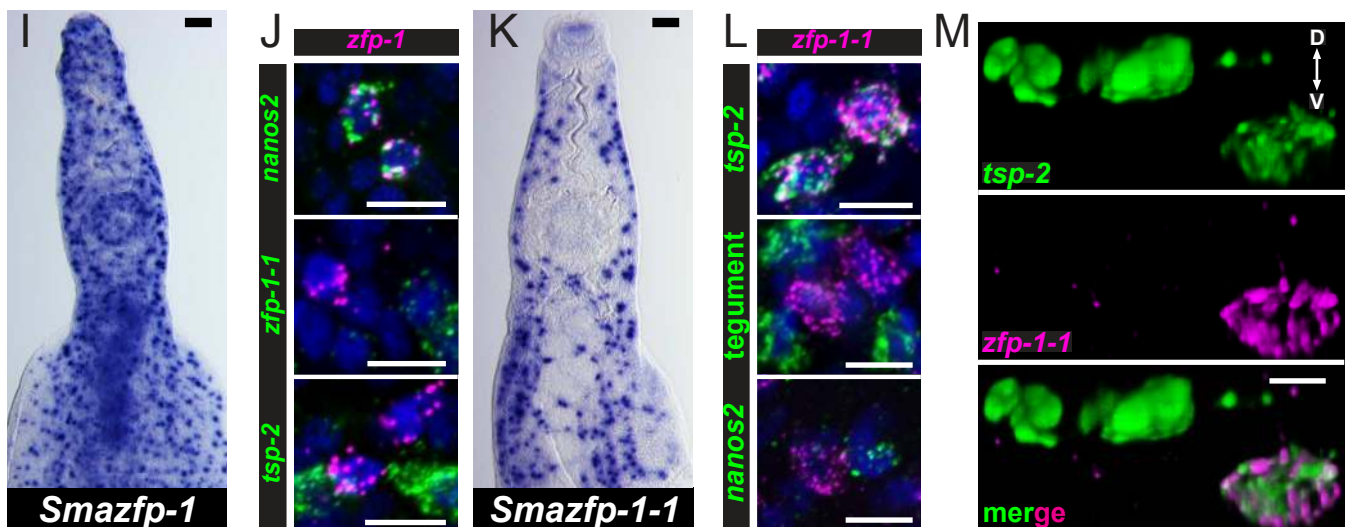
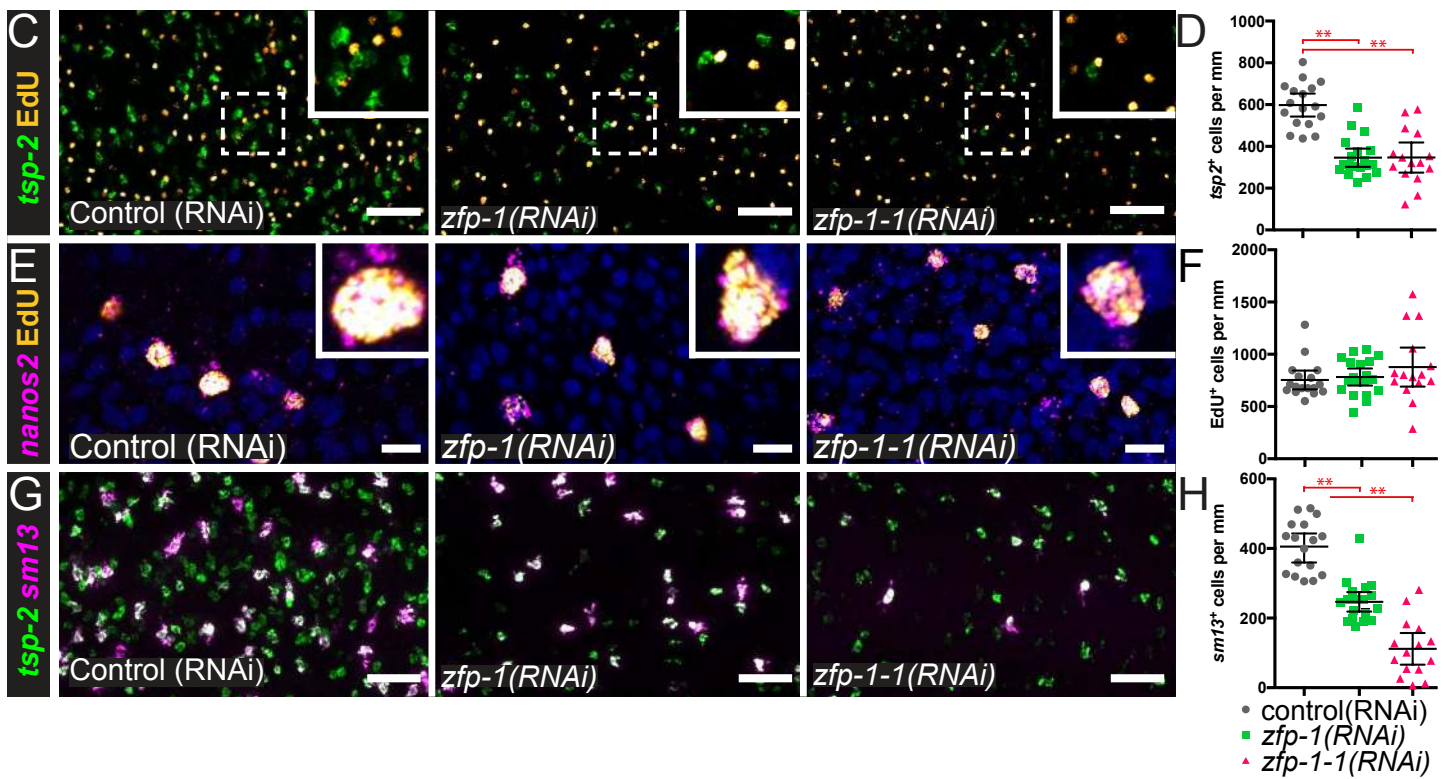
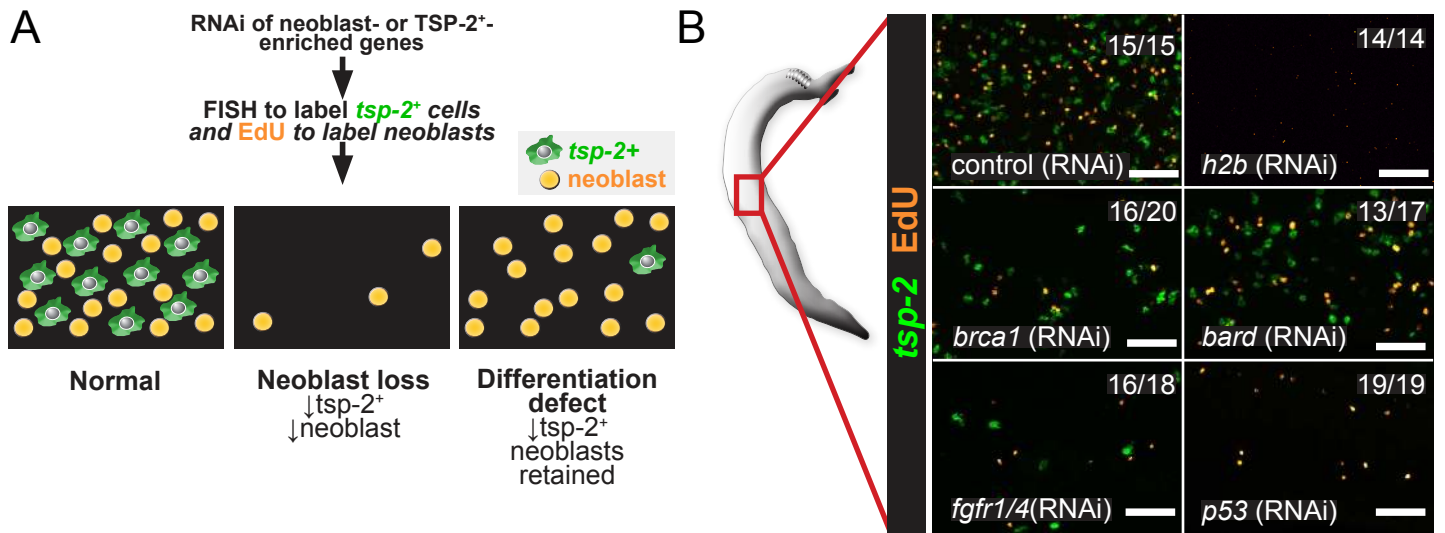


Figure 3-Figure Supplement 1

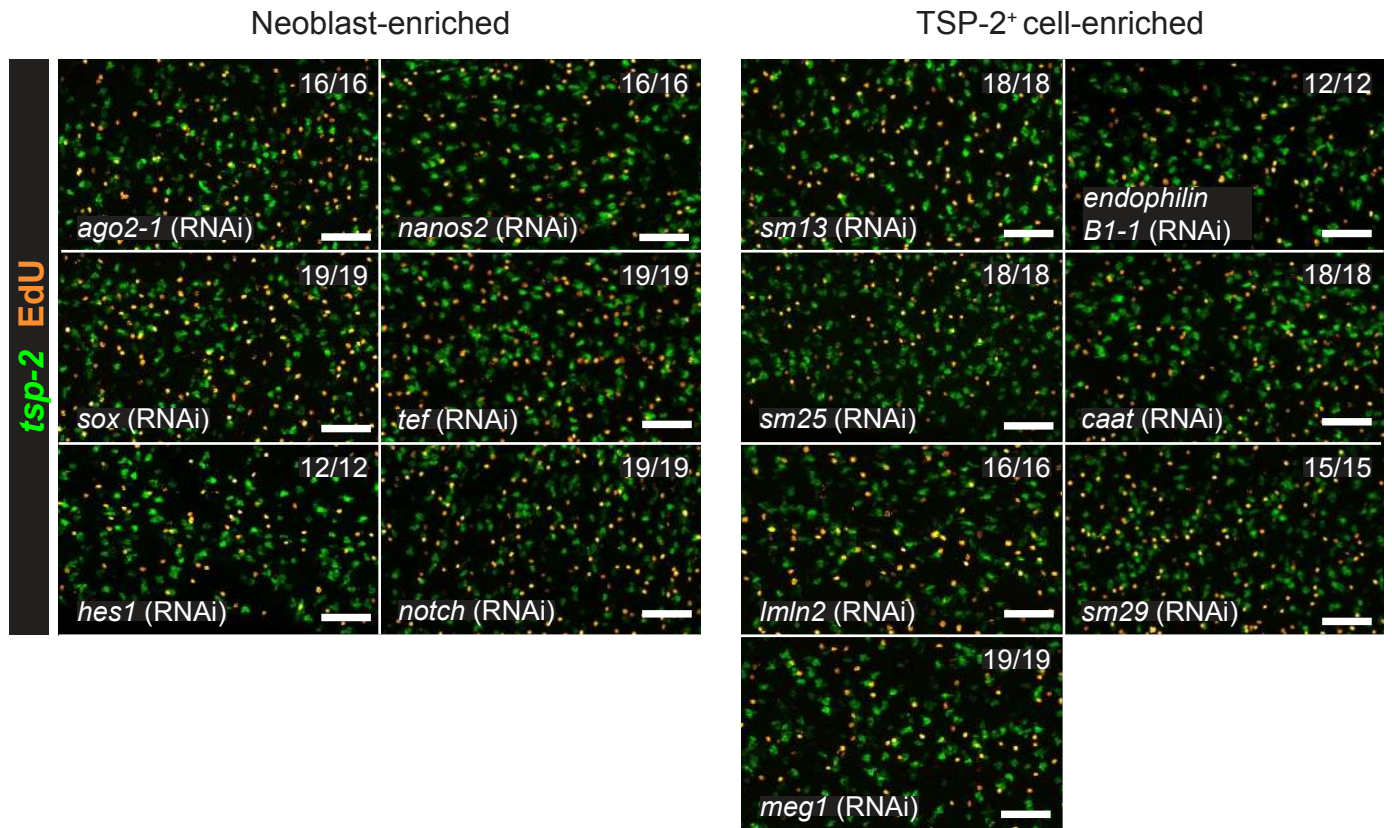


Figure 3-Figure Supplement 2

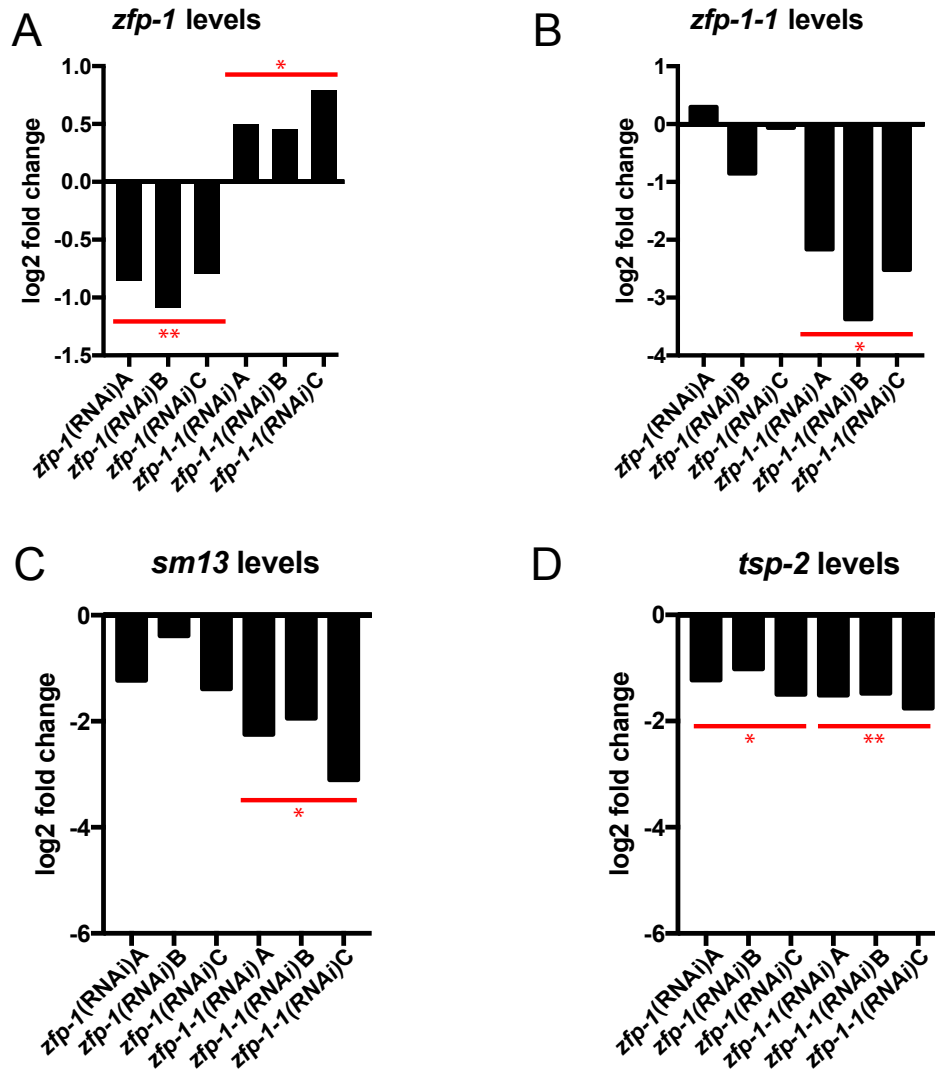


Figure 3-Figure Supplement 3

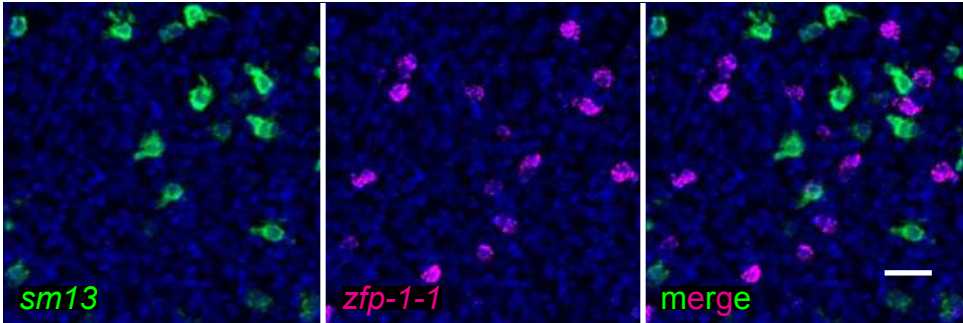
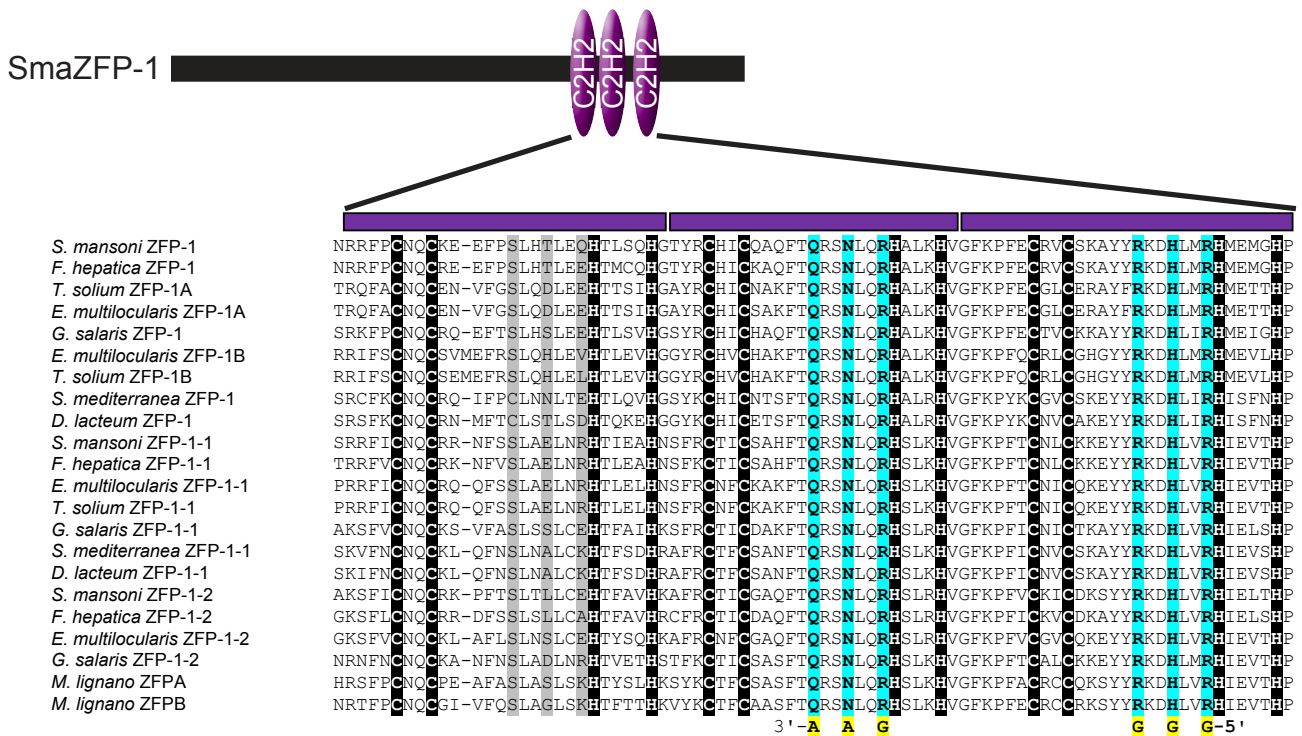
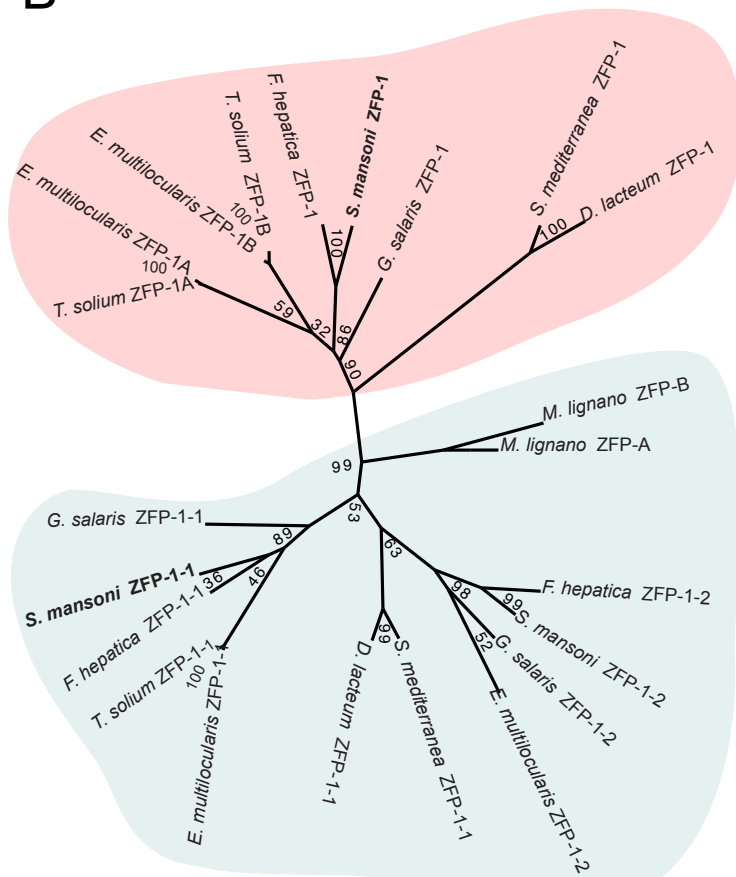


Figure 4

A



B



C

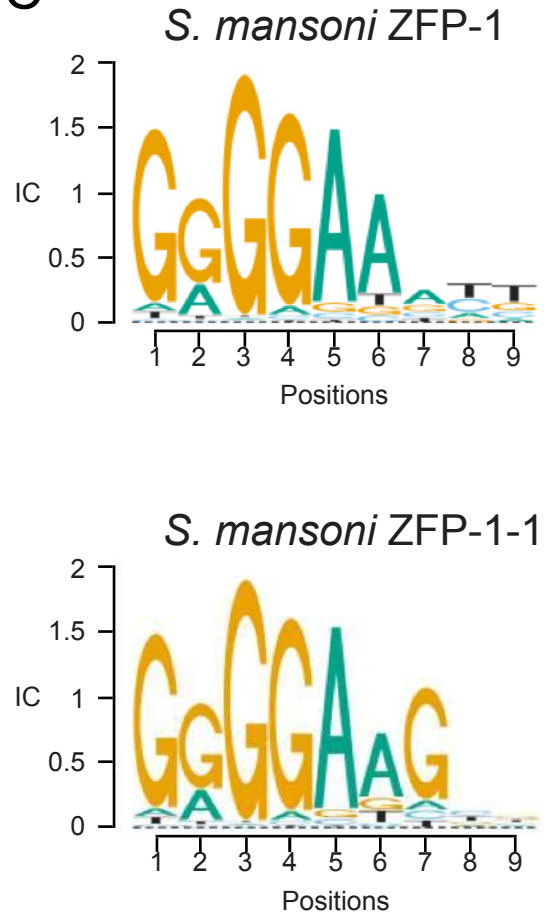


Figure 5

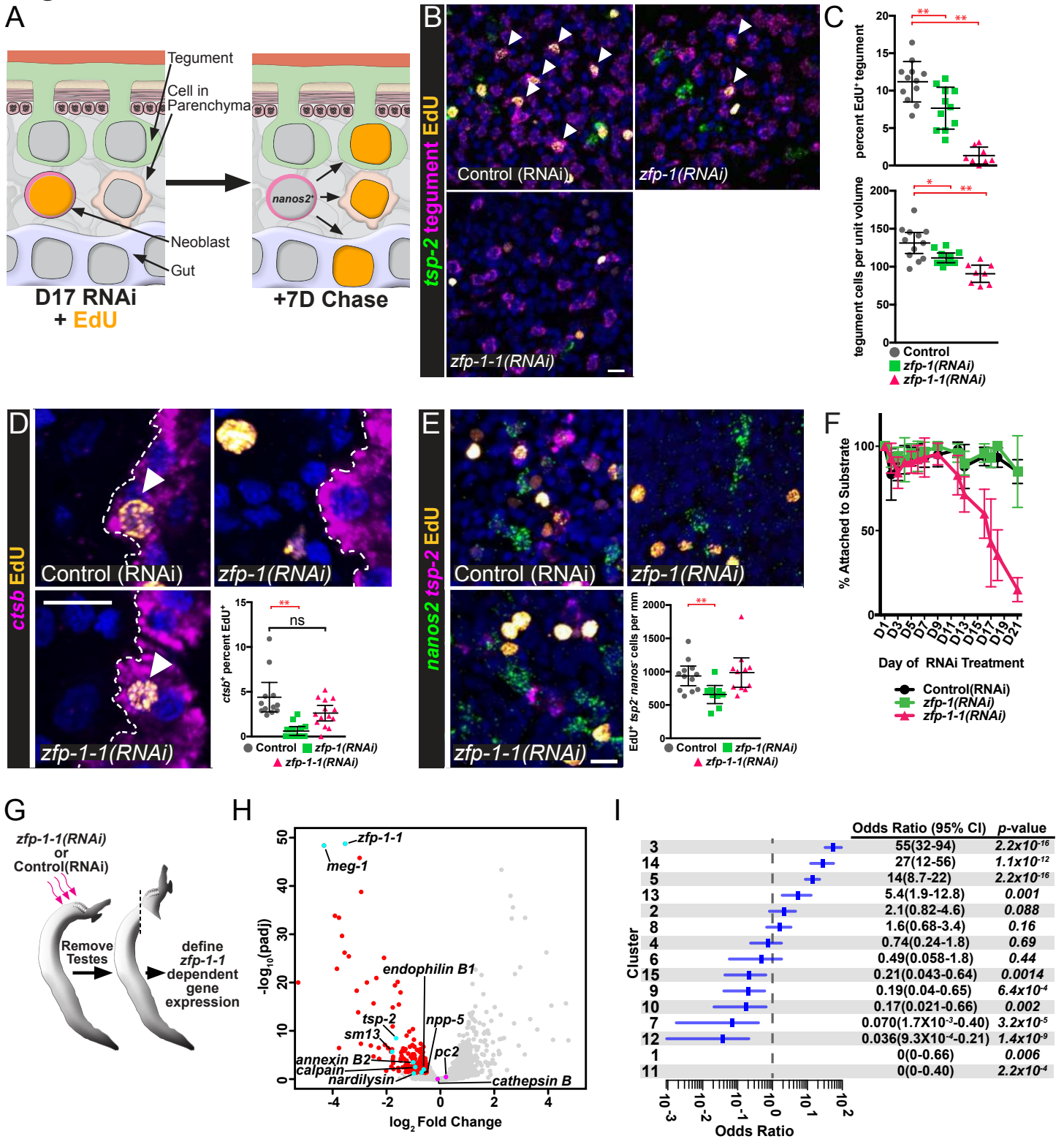


Figure 6

